

# POLITECNICO DI TORINO

Department of Environment, Land and Infrastructure Engineering



MASTER OF SCIENCE IN PETROLEUM AND MINING ENGINEERING

## **The Assessment of Fiber Optic Sensing for the Identification of Three Phase Flow Regimes in Pipelines (Multiphase Flow Metering)**

**Candidate:**

Omar Ali Awad

**Supervisors:**

Prof. Chiara Diangeli

Dr. Aziz Rahman (Texas A&M University)

October 2020

Thesis submitted in compliance with the requirements for the Master of Science degree

## **ACKNOWLEDGEMENTS**

First of all, I would like to thank God, The Almighty, for my success in my educational career and for the completion of my Master's degree.

I would like to acknowledge Dr. Aziz Rahman at Texas A&M University at Qatar for his continuous guidance and patience, and for the T3 Grant of Texas A&M University for providing me the opportunity to work under this project. Also, I would like to thank my Professor Chiara Deangeli for her supervision.

No words can describe my gratitude to my lovely family that supported me throughout my educational journey: my father who has always been my intellectual role model, my mother who was there to encourage me to reach out to my utmost goals, my fiancée who has always believed in my potentials and cherished them, and finally to my brother and sisters who were always caring and considerate. I am proud to have you all in my life.

Thanks to all my friends in Lebanon and Italy for making difficult times proceed smoothly.

Finally, I would like to pass my deep recognition to Politecnico Di Torino along with the Lebanese University for the double degree program that has contributed to my personal growth by gaining valuable educational and life experiences while studying in Italy.

## ABSTRACT

Fiber Optics is an up growing modern technique widely utilized in the oil field. Multi-phase flow metering in pipelines represents an essential objective for Distributed Fiber Optic Sensing (DFOS) techniques. The objective of the work is the explanation of Distributed Acoustic Sensing (DAS) mechanism in multi-phase flow metering with proposing an experimental set up for the mentioned target. Principle of operation of Fiber Optics is explained with the methodology of sensing procedure of each type. Literature survey for previous attempts on this topic is provided. A parametric sensitivity study on the phase fraction obtained from DAS speed of sound measurement is performed to understand physical parameters effect on its behaviour. Proposed experimental multi-phase flow loop for Texas A and M University at Qatar laboratory through a horizontal pipe with ability to incline for 15° based on DAS is presented.

**Keywords:** Multiphase flow; Fiber Optics; Flow metering; Pipeline; Distributed Acoustic Sensing.

# TABLE OF CONTENTS

<b>LIST OF FIGURES</b> .....	<b>viii</b>
<b>LIST OF TABLES</b> .....	<b>x</b>
<b>LIST OF ACRONYMS AND SYMBOLS</b> .....	<b>xi</b>
<b>Chapter 1 : Introduction</b> .....	<b>1</b>
<b>Chapter 2 : Theory</b> .....	<b>4</b>
<b>2.1 Fiber Optic Technology</b> .....	<b>4</b>
<b>2.2 Distributed Fiber Optic Sensing (DFOS)</b> .....	<b>7</b>
2.2.1 Distributed Temperature Sensing (DTS).....	9
2.2.2 Distributed Acoustic Sensing (DAS) .....	12
2.2.3 Distributed Pressure Sensing (DPS).....	14
<b>Chapter 3 : Applications</b> .....	<b>17</b>
<b>3.1 DTS Applications</b> .....	<b>17</b>
3.1.1 Pipeline Leakage Detection .....	17
3.1.2 Real-Time Gas Kick Detection.....	18
3.1.3 Monitoring Acid Stimulation Treatments .....	18
3.1.4 Reservoir Geo-Statistical Description .....	19
3.1.5 Well Bore Monitoring .....	19
3.1.6 Injection and Production Profiling .....	19
<b>3.2 DAS Applications</b> .....	<b>20</b>
3.2.1 Multiphase Flow Metering .....	20
3.2.2 Geophysical Applications.....	20
3.2.3 Hydraulic Fracture Diagnosis.....	21
3.2.4 Sand Detection .....	21

3.2.5 Electric Submersible Pump (ESP) Surveillance.....	22
<b>3.3 Applications of combined DAS and DTS integration.....</b>	<b>22</b>
3.3.1 Gas Lift Surveillance.....	22
3.3.2 Fluid Ingress Position Identification .....	23
<b>3.4 Applications of DPS.....</b>	<b>24</b>
3.4.1 Production Data Analysis.....	24
3.4.2 Near Wellbore Permeability Estimation for Horizontal Well .....	25
<b>Chapter 4 : Literature Review.....</b>	<b>26</b>
<b>4.1 Experimental Papers.....</b>	<b>26</b>
<b>4.2 Modeling Papers .....</b>	<b>29</b>
<b>4.3 CFD Papers.....</b>	<b>32</b>
<b>Chapter 5 : Sensitivity Study on Phase Fraction.....</b>	<b>34</b>
<b>5.1 SoS determination using DAS .....</b>	<b>34</b>
<b>5.2 Utilization of SoS for multiphase flow metering.....</b>	<b>38</b>
5.2.1 Case of single phase flow metering .....	38
5.2.2 Case of two phase flow metering.....	38
5.2.2.1 Liquid-Liquid Flow.....	40
5.2.2.2 Liquid-Gas Flow.....	41
5.2.3 Case of three phase flow metering .....	42
<b>5.3 Sensitivity study on phase fraction of two phase flow.....</b>	<b>44</b>
5.3.1 Case of Liquid-Liquid flow.....	46
5.3.1.1 Oil density effect.....	46
5.3.1.2 Oil Bulk Modulus effect.....	47
5.3.1.3 Pipe diameter effect.....	49
5.3.1.4 Temperature effect .....	50

5.3.1.5 Pipe thickness effect.....	52
5.3.1.6 Pipe Young's modulus of elasticity effect .....	53
5.3.2 Case of Liquid-Gas flow.....	53
5.3.2.1 Oil density effect.....	54
5.3.2.2 Temperature effect .....	55
<b>Chapter 6 : Proposed Experimental Setup.....</b>	<b>57</b>
<b>6.1 Objective.....</b>	<b>57</b>
<b>6.2 Experimental Setup.....</b>	<b>57</b>
<b>6.3 Operating conditions of the system.....</b>	<b>59</b>
<b>6.4 Description of experimental components.....</b>	<b>59</b>
6.4.1 Annulus System.....	59
6.4.2 Pump .....	60
6.4.3 Tank.....	61
6.4.4 Motor .....	62
6.4.5 Fiber Optic Cable.....	62
6.4.6 iDAS .....	62
6.4.7 Flow meters .....	63
6.4.7.1 Liquid flow meter .....	63
6.4.7.2 Gas flow meter .....	63
6.4.8 Eccentricity Regulator.....	63
6.4.9 Air Supply Line.....	63
6.4.10 Hydrocyclone.....	63
<b>6.5 Risk Analysis.....</b>	<b>65</b>
<b>Chapter 7 : Conclusion .....</b>	<b>79</b>
<b>7.1 Discussion and Conclusion .....</b>	<b>79</b>

<b>7.2 Future Work Recommendations .....</b>	<b>80</b>
<b>References .....</b>	<b>81</b>

## LIST OF FIGURES

Figure 2.1: Showing Total internal reflection. ....	5
Figure 2.2: Top view of the four components of fiber optic structure [9]. ....	5
Figure 2.3: Size of the dimensions of both types of fiber optic, single mode and multimode [9]. ....	7
Figure 2.4: Main groups of fiber optic sensors [10]. ....	7
Figure 2.5: Difference between distributed and non-distributed sensing [16]. ....	8
Figure 2.6: Different scattering bands used for DFOS [20]. ....	10
Figure 2.7: DTS configuration system. ....	11
Figure 2.8: Operation principle of DAS [29]. ....	13
Figure 2.9: Strain (Radial and Axial) induced by applied pressure [33]. ....	15
Figure 2.10: Fiber optic pressure sensing system [33]. ....	15
Figure 3.1: Figure showing DTS system for leak detection [37]. ....	18
Figure 3.2: Micro-seismic event monitored by Geophone (red colour) and DAS system (grey colour) [8]. ....	21
Figure 3.3: Flow chart of DAS data analysis mechanism [48]. ....	23
Figure 3.4: Plot showing flow contribution versus Hydraulic fracture half-length [50]. ....	24
Figure 3.5: Flow chart showing effects of increasing noise level [51]. ....	25
Figure 5.1: Acoustic field along total length of pipe. ....	34
Figure 5.2: Sound waves in opposite directions of flow. ....	35
Figure 5.3: Backscattered signal due to acoustic field effects. ....	35
Figure 5.4: Depth-Time curve from DAS data [4]. ....	36
Figure 5.5: 2D Fourier transform of DAS data [4]. ....	37

Figure 5.6: Typical SoS curve function of WLR in Oil/Water flow [2].	41
Figure 5.7: Typical SoS curve function of HL in Oil/Gas flow [2].	42
Figure 5.8: Typical SoS curve function of Mixture Density in Water/Oil/Gas flow [2].	43
Figure 5.9: Differential pressure sensor configuration [5].	44
Figure 5.10: Oil density effect on WLR curve versus SoS.	47
Figure 5.11: Oil Bulk Modulus effect on WLR curve versus SoS.	48
Figure 5.12: Pipe diameter effect on WLR curve versus SoS.	49
Figure 5.13-A: Dispersed oil in water flow in pipeline.	50
Figure 5.13-B: Stratified oil-water flow in pipeline.	50
Figure 5.14: Temperature effect on WLR curve versus SoS.	51
Figure 5.15: Pipe thickness effect on WLR curve versus SoS.	52
Figure 5.16: Pipe Young's modulus of elasticity effect on WLR curve versus SoS.	53
Figure 5.17: Oil density effect on WLR curve versus SoS.	54
Figure 5.18: Temperature effect on WLR curve versus SoS.	56
Figure 6.1: Schematic representation of multiphase flow loop.	58
Figure 6.2: Dimensions of aluminium frame (in mm).	60
Figure 6.3: Tank design and specifications.	61
Figure 6.4: iDAS picture [58].	62
Figure 6.5: Hydrocyclone design specifications.	64

## LIST OF TABLES

Table 2.1: Summary of different DFOS techniques.....	16
Table 4.1: Experiments using DFOS for multiphase flow metering. ....	26
Table 4.2: Summary of Modelling DFOS for multiphase flow metering. ....	29
Table 4.3: CFD papers using DFOS for multiphase flow metering.....	32
Table 6.1: Likelihood standards. ....	65
Table 6.2: Severity of consequences standards.....	66
Table 6.3: Risk Matrix.....	67
Table 6.4: Risk acceptance criteria. ....	67
Table 6.5: HAZOP on Node 1. ....	69
Table 6.6 HAZOP on Node 2. ....	71
Table 6.7: HAZOP on Node 3. ....	72
Table 6.8: HAZOP on Node 4. ....	73
Table 6.9: HAZOP on Node 5. ....	74
Table 6.10: HAZOP on Node 6. ....	75
Table 6.11: HAZOP on Node 7. ....	76
Table 6.12: HAZOP on Node 8. ....	77

## LIST OF ACRONYMS AND SYMBOLS

DFOS	Distributed Fiber Optic Sensing
DTS	Distributed Temperature Sensing
DAS	Distributed Acoustic Sensing
DPS	Distributed Pressure Sensing
OTDR	Optical Time Domain Reflectometry
OFDR	Optical Frequency Domain Reflectometry
ESP	Electrical Submersible Pump
CFD	Computational Fluid Dynamics
PDF	Probability Density Function
SoS	Speed of Sound
WLR	Water in Liquid Ratio
HL	Liquid Holdup
HAZOP	Hazard and Operability Study

# Chapter 1: Introduction

Multiphase flow can be defined as the simultaneous flow of fluids with two or more phases; it is the common type of flow present in different oil field sectors, including drilling, production, and transportation. The understanding of multiphase flow in pipelines requires diving through two fundamental approaches: the first is the characterisation of flow through determining flow rates of individual phases, and the second is the flow composition determination. The obstacle of absence of clear numerical model through equations and conditions that can solve any multiphase flow circumstances continues to raise new challenges in this field. With such wide presence of multiphase flow in oil field like gas/oil, water/gas, oil/water/gas or other flow compositions even with sand particles, it is essential to study this type of flow and characterize its thermodynamical and physical parameter variations for several purposes such as injection and production profiling, downhole monitoring, and building wellbore model simulations. The techniques used for this objective differ with the competition for the most feasible-efficient method. With the beginning of the 1990's a new technology was present in the oil field for numerous applications achieving optimal operating conditions, which is the Fiber Optic technology.

Variation in physical parameters such as density or velocity play a major rule in the transition of the type of flow in pipeline, which is defined as the flow regime or flow pattern such as bubbly, slug, churn, or dispersed flow. Understanding the evolution of different flow regimes require multiphase flow metering, the objective of the work is to understand why and how distributed fiber optic sensing is used for flow metering, particularly the Distributed Acoustic Sensing (DAS) mechanism is explained, and finally proposing an experimental setup to apply it for multiphase flow metering using DAS.

The present study provides parametric sensitivity study for both cases of phase fraction (liquid-liquid flow and liquid-gas flow), to provide a clear qualitative analysis on the effect of physical parameters of both fluid and pipeline on phase fraction behaviour. For practical implementation of Distributed Acoustic Sensing, the present study contains a design of an experimental setup for a multiphase flow loop.

The fiber optic technology was implemented due to its unique properties such as flexibility, distributed sensing, fast data transmission through long distances, and layered structure ensuring mechanical protection for harsh environmental conditions that suits oil field environments as an efficient sensing technique, through several experimental and field trials, it was proven the efficiency for this technique to monitor and characterize multiphase flow in pipelines either for transportation or in production/injection operations [1] [2] [3] [4].

In this study, firstly, in chapter 2 the fiber optic technology is discussed in details by explaining its characteristics, principle of operation, and method of classification. Followed by introducing the concept of distributed fiber optic sensing (DFOS) and the functioning mechanism of its three main types (DAS-DTS-DPS) showing the differences between Rayleigh, Raman, and Brillouin scattering techniques that each type is based on respectively [2] [5].

To show the up growing importance of fiber optics in oil field and the reasons behind their increasing usage, chapter 3 was allocated to applications in oil field of all three types of distributed fiber optic sensing technique such as multiphase flow metering, injection monitoring, sand detection, hydraulic fracture monitoring and many other important applications [6] [7] [8], also applications including the integration of more than one type in the same system were indicated.

A literature survey on previous publications on multiphase flow metering and flowregime identification using optic fibers was done in chapter 4, where it was divided into three main categories: Experimental-Modelling-Computational Fluid Dynamics.

Chapter 5 was devoted for clarification of Speed of Sound SoS determination procedure from DAS, showing how to obtain SoS and implementing it in multiphase flow to obtain the key to resolve the flow through determination of both phase fraction and flow rate of each individual phase, eventually sensitivity study was performed on several parameters including density, bulk modulus, pipe diameter, pipe thickness and temperature to understand and discuss the behaviour of the phase fraction correlated from SoS.

Due to the world wide Covid-19 emergency, we were not able to perform the experiment of DAS in a multiphase flow lab in Texas A and M University at Qatar, so we were satisfied with a proposed experimental setup and DAS implementation on the design in chapter 6, the multiphase loop was designed to introduce DAS technology to an experimental identification of multiphase flow regimes with a three phase with a detailed specifications on chosen components, the proposed setup takes into consideration inclination effects (maximum of 15 degree with horizontal). Hazard and Operability Study (HAZOP) is performed on the system to apply a risk analysis to different components of the system securing a safe design.

Finally, In the last chapter, the results and the method are discussed.

## Chapter 2: Theory

This section provides the theory behind fiber optic technology and its classification. Then a detailed explanation of distributed fiber optic sensing, and the principle of operation of each of its three main types is presented.

### 2.1 Fiber Optics Technology

Fiber optics is a modern technology that uses a strand of fibers fabricated from glass to transmit data as a pulse of light covering long distances. The main principle governing the operation of fiber optics is “Total Internal Reflection”. The design of the fiber must achieve disparity in the index of refraction between the core with higher refractive index-carrying the light- and the cladding surrounding the core part with lower refractive index. The critical angle  $\theta_c$  is an angle of incidence resulting in a  $90^\circ$  angle of refraction, according to Snell’s law (Equation 2.1):

$$n_1 \sin \theta_1 = n_2 \sin \theta_2 \quad (2.1)$$

Where  $n_1$  and  $n_2$  are the refractive indices of medium 1 and 2 respectively, and  $\theta_1$  is the angle of incidence,  $\theta_2$  is the angle of refraction. We can calculate the critical angle by giving the angle of refraction a value of  $90^\circ$ , thus  $\theta_c$  is given by (Equation 2.2):

$$\theta_c = \arcsin\left(\frac{n_2}{n_1}\right) \quad (2.2)$$

When the incident light ray hits with  $\theta_i > \theta_c$  it will be totally reflected (green colour) back to the core and will not proceed to the next medium(cladding) as shown in figure 2.1.

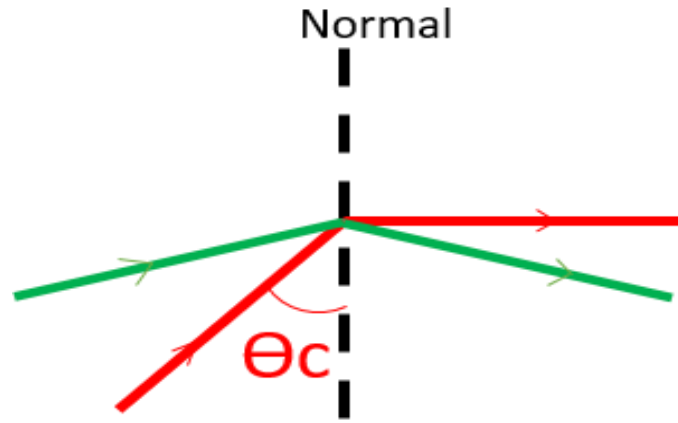


Figure 2.1: Total internal reflection.

Figure 2.2 presents the different parts or components forming the optical fiber, these include:

- Core: The central component with cylindrical geometry transmitting light signals, usually made from glass.
- Cladding: Layer encircling the core section, ensuring total internal reflection of light signals so they are not exiting the fiber due to its lower refractive index.
- Buffer: The layer responsible for protecting the cladding by absorbing shocks or any other physical damage.
- Jacket: According to the jacket colour we can identify the fiber optic cable category that means the type (single mode or multi-mode).

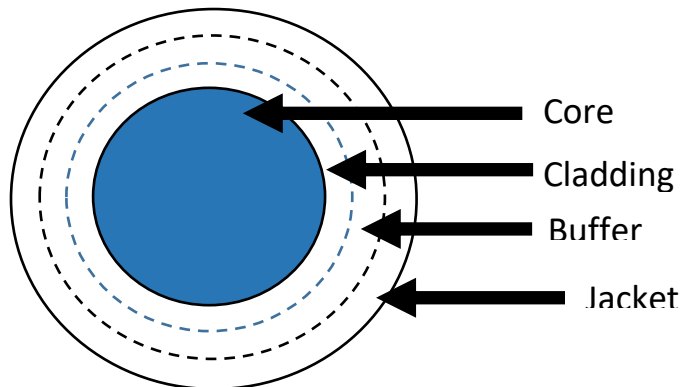


Figure 2.2: Top view of the four components of fiber optic structure [9].

Optical fibres are divided into several categories according to their objective, hence it is essential to comprehend the properties of fiber optics to comprehend their employment [10]. Most famous grouping is done according to the mode number, into single mode and multi-mode as shown in figure 2.3.

- Multi-mode fiber: This type of optical fibers is designed with a core of big diameter-compared to single mode fiber-between 50-62.5  $\mu\text{m}$  to carry multiple light rays with different angles of reflection in the core. The main employment of this class of fibers is short length transmission used in video surveillance, network systems, and other communication purposes [11].
- Single mode fiber: On the contrary, prolonged length communications require the usage of this type including telephone or TV transmission systems. They are designed with small core diameter with 5-10  $\mu\text{m}$ , noting that both types of fiber optics share the same cladding diameter that is 125  $\mu\text{m}$ .

Light passes through the core parallel to the core axis of the fiber due to the small size of the diameter, hence less attenuation is formed and light can transfer along the prolonged distances. The required constrain allowing passage of light for single mode fibers is having the normalized frequency  $v < 2.405$ , otherwise higher values of normalized frequency refer to multi-mode fibers [12].  $v$  is a dimensionless number defined by (Equation 2.3):

$$v = \frac{2\pi a}{\lambda} \sqrt{n_1^2 - n_2^2} = \frac{2\pi a}{\lambda} NA \quad (2.3)$$

Where  $a$  is the fiber core diameter,  $\lambda$  is the light propagation wavelength,  $n_1$  is the refractive index of the core and  $n_2$  is the refractive index of the cladding, and  $NA$  is the numerical aperture by applying its concept [13].

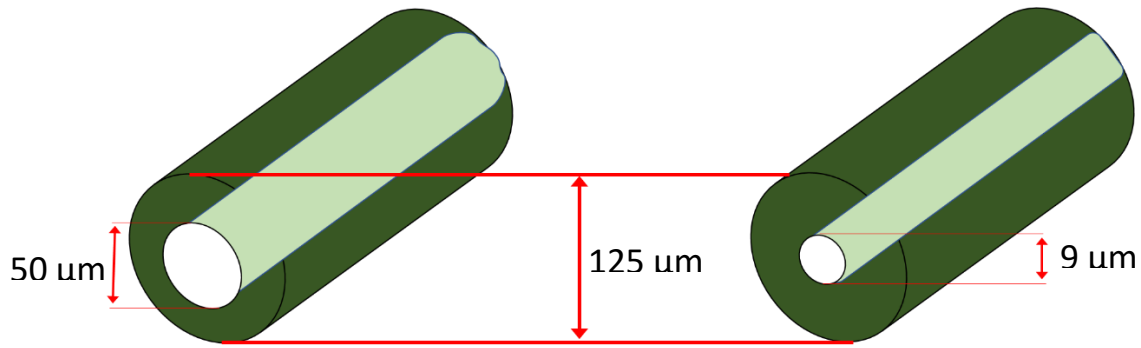


Figure 2.3: Size and dimensions of both types of fiber optic, single mode and multimode [9].

## 2.2 Distributed Fiber Optic Sensing (DFOS)

DFOS is one of three different groups of fiber optic sensing where each group is designed based on the desired objectives and parameters/measurements of desire, figure 2.4 classifies the different groups with the major types of each group [10].

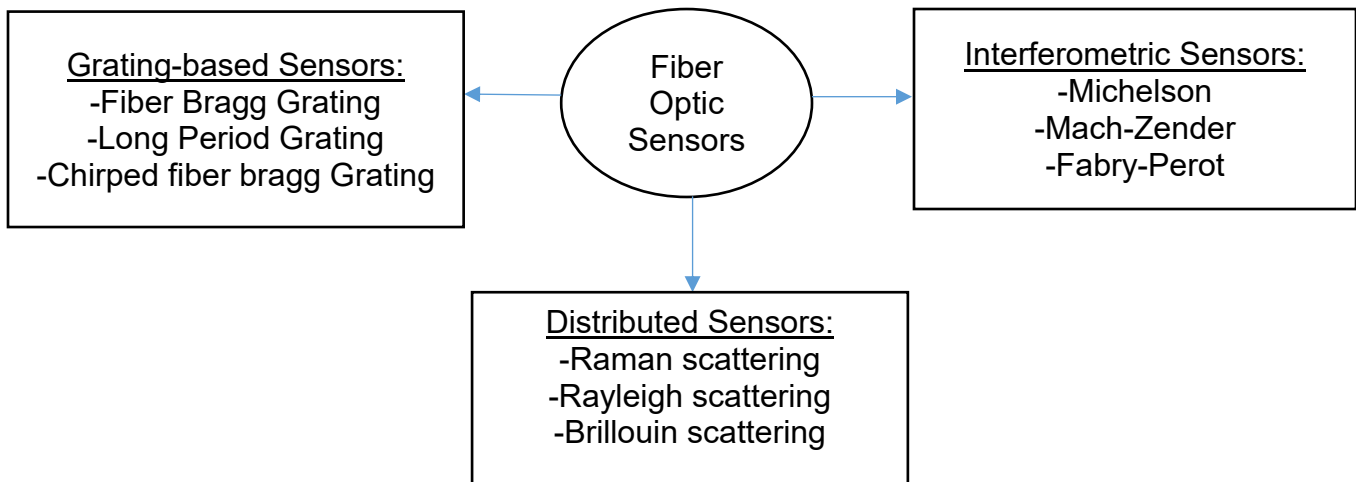


Figure 2.4: Main groups of fiber optic sensors [10].

The main interest in our research is DFOS which will be discussed in further details. This concept of distributed sensing is mainly referring to transmitting huge amounts of data to long distances minimizing the data loss, and covering the whole distance by producing a continuous profile of the measured parameter which gives it an advantage over other techniques as shown in figure 2.5. DFOS involves the transformation of the fibers to an optoelectronic sensor either as an extrinsic sensor or intrinsic sensor. Extrinsic sensors play the role of an advisor which advises the light from the source of light towards the optical sensor head then towards the photo detector; light ray will either exit the fiber and thus be cached by a barrier or be reflected in the same fiber to reach the detector. On the other hand, in intrinsic sensors the light will not escape from the fiber giving an advantage of resistance to both electromagnetic interference and harsh environmental conditions that can have harmful effects on extrinsic sensors [14] [15].

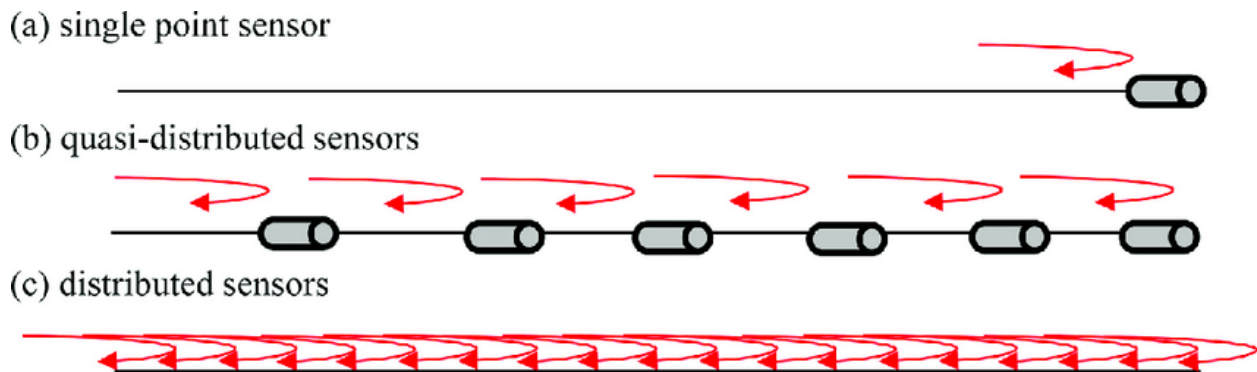


Figure 2.5: Difference between distributed and non-distributed sensing [16].

Indicating the position at which the measured parameter is monitored can be done using the Optical Time Domain Reflectometry (OTDR) or Optical Frequency Domain Reflectometry (OFDR). Which is based on measuring the time the backscattered signal takes to enter the photo detector. Optical Time Domain Reflectometry (OTDR) is about measuring the time the incident signal took to be backscattered to detection unit (where reflected power decreases over time) thus identifying the location of the measurand along the length of the fiber.

The following section explains the mechanism of the three types of optic distributed sensing.

### **2.2.1 Distributed Temperature Sensing (DTS)**

DTS allows to obtain the continuous profile of temperature along the length of fiber cable that can cover several kilometres with high accuracy and spatial resolution with 1m, several experimental studies have been applied to prove the high accuracy of such sensing technique, a companion paper proved after optimization that accuracy of results can reach less than 1°C for a distance of 10.8 km [17].

DTS technique is based on one of three principles of back scattered light detection involving Rayleigh, Raman, or Brillouin scattering [10]. The illustration of these concepts:

#### ***Raman Scattering technique:***

Optical fibers are fabricated from doped quartz glass, an arrangement of Silicon dioxide (SiO<sub>2</sub>) which are sensitive to several physical quantities including temperature, since the thermal ramifications will induce variations in transmission properties inside the fibers by creating oscillations in the core. Thus when the light ray propagates in the medium and feels the thermal changes, a light scattering called Raman scattering occurs due to the interaction between photons of light from one side and the electrons from molecules affected by the oscillation from another. Scattered light ray is dissimilar to the incident ray, since it experiences a spectral shift identical to the resonance frequency resulting from the oscillation [18].

The scattered light ray can be divided into three constituents shown in figure 2.6 which are:

- Rayleigh scattering: This is the spectral constituent with wavelength equal to the laser source.
- Stokes constituent: Made up from photons shifted with a greater wavelength or lower frequency.

- Anti-Stokes constituent: Initiated from photons shifted with a shorter wavelength or greater frequency, and is temperature related unlike Stokes line.

Local temperature is obtained from the ratio of Anti-Stokes and Stokes rays intensities [19].

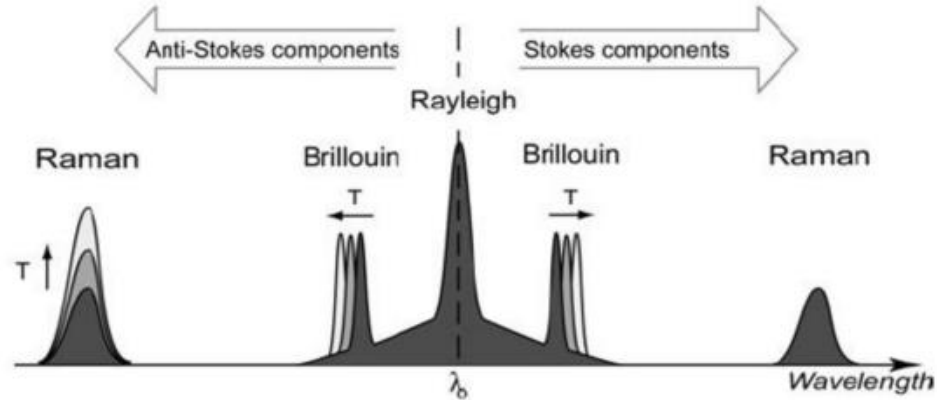


Figure 2.6: Different scattering bands used for DFOS [20].

The formula expressing the relationship between the ratio  $R(T)$  of intensities and temperature is given by (Equation 2.4):

$$R(T) = \frac{I_s(T)}{I_{As}(T)} = \left( \frac{V_0 + V_V}{V_0 - V_V} \right)^4 * \exp\left(-\frac{h * \Delta V}{K * T}\right) \quad (2.4)$$

Where  $I_s(T)$  and  $I_{As}(T)$  are the intensities of Stokes and Anti-Stokes respectively,  $V_0$  and  $V_V$  are the frequencies of laser source and vibrational transition,  $h$  is the Planck's constant,  $\Delta V$  is the Raman frequency shift,  $T$  is the temperature,  $K$  is the Boltzmann's constant [21].

Figure 2.7 shows a typical DTS configuration system. Light ray is generated from the laser source and guided through the fiber optic sensor, when the measured parameters effects which are the thermal effects in this case starts affecting the properties of transmitted light, a back scattered ray is reflected in the fiber and guided toward signal processing unit, thus the temperature is determined (Equation 2.4) at any position of desire referring to the OTDR or OFDR principle [22].

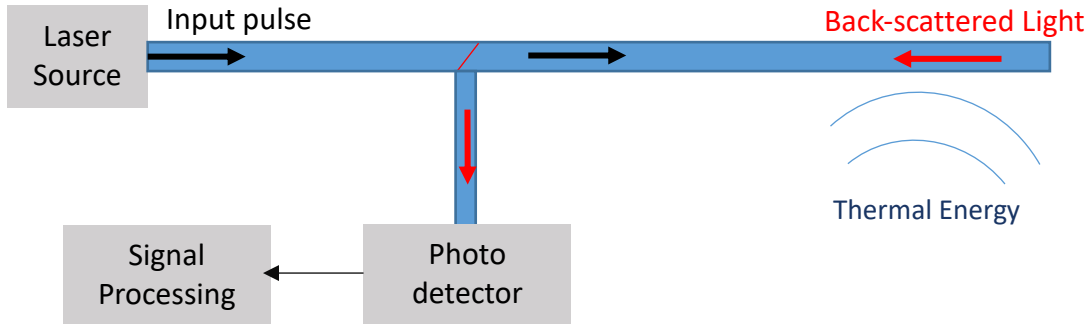


Figure 2.7: DTS configuration system.

**Brillouin Scattering technique:**

When an interaction occurs between the acoustic phonons in the medium and an acoustic wave leading to scattering of light wave, this interaction is classified as inelastic [23]. The Brillouin scattering generates two opposite modes of frequency shift, the first increasingly shifting which is Anti-Stokes light and the second decreasingly shifted called Stokes, the formula governing the frequency shift is (Equation 2.5):

$$\nu_b = \frac{\omega_b}{2\pi} = \frac{2n\nu_a}{\lambda_L} \quad (2.5)$$

Where  $\nu_b$  represents the Brillouin frequency shift,  $\omega_b$  is angular frequency shift,  $n$  is the refractive index of the fiber,  $\nu_a$  is the longitudinal acoustic velocity, and  $\lambda_L$  is the free space wavelength of the pump light [24]. The frequency shift of Brillouin scattering is linearly dependent with both temperature and strain as shown in [24], formulated by(Equation 2.6):

$$\partial\nu_b = C_{\nu\varepsilon}\partial\varepsilon + C_{\nu\theta}\partial\theta \quad (2.6)$$

$C_{v\varepsilon}$  and  $C_{v\theta}$  represent the coefficients of Brillouin shift due to strain( $\varepsilon$ ) and temperature( $\theta$ ) respectively. In the case of applying  $\lambda_L=1.55 \mu\text{m}$  both coefficients can be monitored as  $C_{v\varepsilon} = 0.048 \text{ MHz} / \mu\text{m}$  and  $C_{v\theta} = 1.1 \text{ MHz} / \text{K}$  [25].

The proceeding illustration shows the capability of Brillouin scattering to measure either temperature or strain but not both at the same time.

In the 1990's this technique was improved, and both Brillouin OTDR [26] and Brillouin OFDR [27] are studied.

### ***Rayleigh scattering technique:***

This technique is different compared to the previous cases and generally not used for DTS, however it was used in order to monitor the temperature in a nuclear reactor where 2m long single mode fiber optic cable achieved accurate results with accuracy = 0.6% [28].

## **2.2.2 Distributed Acoustic Sensing (DAS)**

DAS is considered a passive sensing technique which is capable of monitoring the acoustic field at any position along the fiber optic cable giving a continuous profile along the whole length at the same time. Many positive characteristics such as compressed spatial resolution that can reach 1 m, notably high frequency sampling rates of magnitude 10 kHz, and enhanced signal to noise ratio show the efficiency of this sensing technique. DAS can also be classified a dynamic strain sensor due to the fact that it is monitoring strain variations along the length of the fiber. When an acoustic wave strikes the fiber at a specified position on the fiber, the pressure pulse of the wave creates tiny strain effects on micro level. Generally for the implementation of DAS system, the single mode fibers are used instead of multimode fibers making use of the single mode of light transmission that can ensure coherency between wave packets and ensuring higher resolution. Figure 2.8 describes the operation principle of DAS. A first light pulse is sent from the laser source through the fiber optic, it undergoes a backscattering phenomenon where the signals S1 and S2 in the blue colour represent the unstrained signals at the start and end of the gauge length respectively, note that

the gauge length is the length between two positions near a DAS channel. Regarding the next light emission, where the condition of the fiber optic was transformed from unstrained to strained, a new couple of signals backscattered from the gauge length named  $S1'$  and  $S2'$ , the concept of DAS is to measure the phase modulation between signals, since the phase lag between summation of  $S1+S2$  and  $S1'+S2'$  is proportional to the strain formed due to acoustic waves on the fiber producing a continuous profile along the fiber length [29].

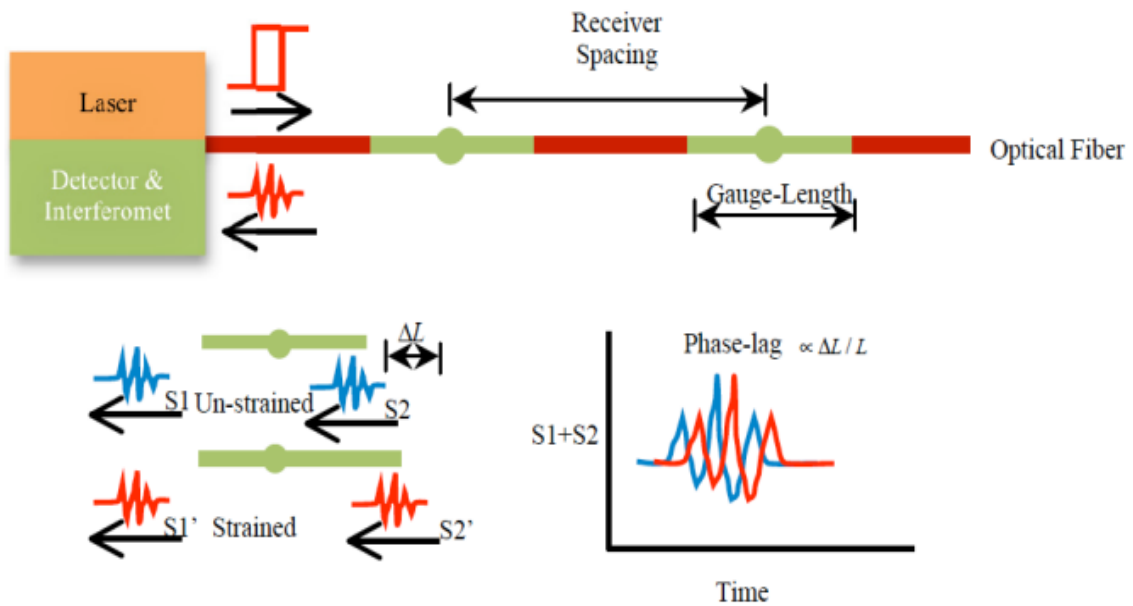


Figure 2.8: Operation principle of DAS [29].

As mentioned previously, for distributed sensing measurements we have three different scattering techniques (Raman-Rayleigh-Brillouin), the Rayleigh scattering which is not characterized by any frequency shift is utilized for DAS [30].

Coherent OTDR concept is the basis of the DAS monitoring, where a light pulse is transmitted along the fiber that undergoes a backscattering due to the acoustic field interaction resulting in small vibrations [31]. The backscattering light intensity and local phase which are sensitive to the vibrations thus formed, thus they can be monitored to obtain continuous acoustic profile along the optical fiber [32].

### 2.2.3 Distributed Pressure Sensing (DPS)

DPS is an important technique that is utilized in many domains including industrial, civil, and oil domain such as monitoring any crippling or leakage in the pipes transporting hydrocarbons.

Description of operating mechanism of DPS starts with the fact that any pressure applied on the fiber optic will cause a formation of a mechanical strain as shown in figure 2.9, that can be axial or radial due to the forces that are either compressive or tensile. The created strain is proportional to the pressure applied on the fiber. Based on the "Photo-Elastic Effect" a variation in the refractive index of the core will be noticed, incident light will undergo Brillouin scattering resulting in back scattered portion of the light with a frequency shift proportional to the strain (as the strain increases a bigger shift is formed) described by a coefficient  $C_{\nu\varepsilon} = 0.048 \text{ MHz}/\mu\text{m}$  for wavelength of incident light  $\lambda_L = 1.55 \mu\text{m}$ , but still noting that the formed spectral shift is due to both thermal and strain effects. This issue can be solved with by utilizing another fiber optic cable that is sequestered from pressure to identify temperature contribution. Brillouin OTDR concept is used to identify the position of strain along the total distance and thus obtaining a continuous profile in real time [33].

Other techniques were applied using Brillouin OFDR but was faced by low pressure sensitivity and by narrowed monitoring length respectively [34].

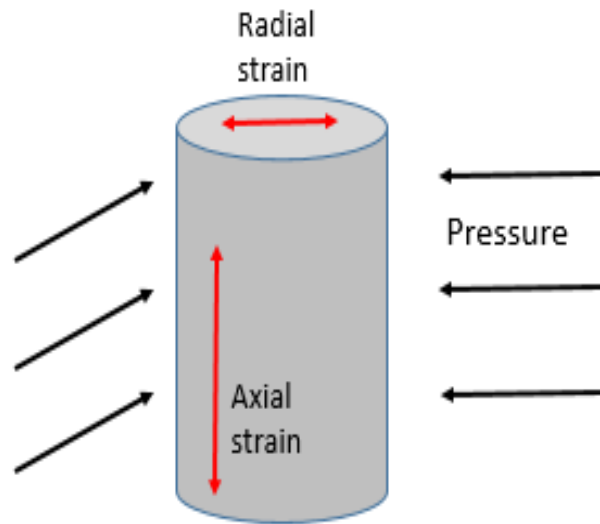


Figure 2.9: Strain (Radial and Axial) induced by applied pressure [33].

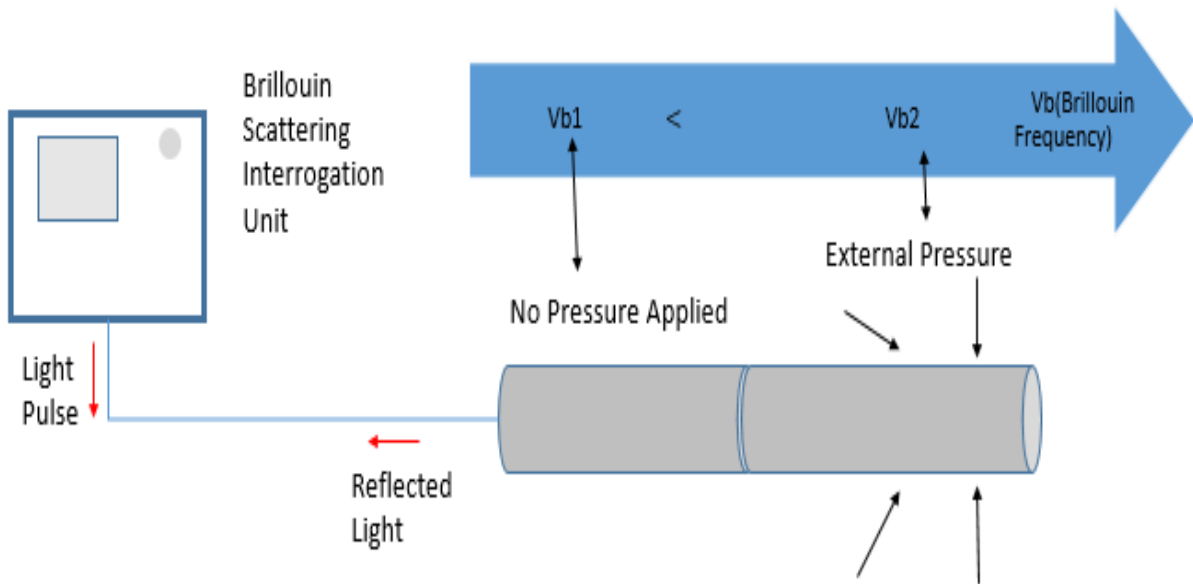


Figure 2.10: Fiber optic pressure sensing system [33].

As a summary of the three previous techniques, the following Table 2.1 describes both the parameters measured for the backscattered signal and the parameters resulting as a physical output from each type of distributed sensing.

<b>Type of DFOS</b>	<b>Light Scattering technique</b>	<b>Optical measurands</b>	<b>Physical Outputs</b>
DTS	Raman	Amplitude of Stokes and Anti-Stokes intensities	Temperature
DAS	Rayleigh	Amplitude and Phase	Dynamic strain and Temperature
DPS	Brillouin	Amplitude and Frequency	Strain and Temperature

Table 2.1: Summary of different DFOS techniques.

# Chapter 3: Applications

There are a variety of applications where DFOS are utilized, especially in the oil industry where the need of discovering more profitable and efficient sensing techniques is continuously required. The following section will discuss several aspects of such applications in the oil and gas industry.

## 3.1 DTS Applications

### 3.1.1 Pipeline Leakage Detection

DTS systems are used to detect any leakage occurring in a pipeline for long distances that can cover 40 km [35]. Usually the detection length is restricted to around less than 50 km, however it still can be expanded through several operations including the utilization of powered electrical amplifier improving or magnifying the signal [36].

The leak detection mechanism is simple, where the flowing matter transported leaks outside the pipeline undergoes direct contact with the DTS system that will monitor a thermal variation from the temperature inside the pipe which can be noticed by the control system, and occurring to the OTDR principle we can define the precise position of the leakage in order to take immediate actions. Privileges of such distributed system include high resolution with less than  $0.01^{\circ}\text{C}$  and the ability to define exact position with 1-5 m along more than 50 km with fast monitoring duration( <10 seconds), flexibility, durability, high power, and the no need to be maintained shows priority on other techniques [37] [20].

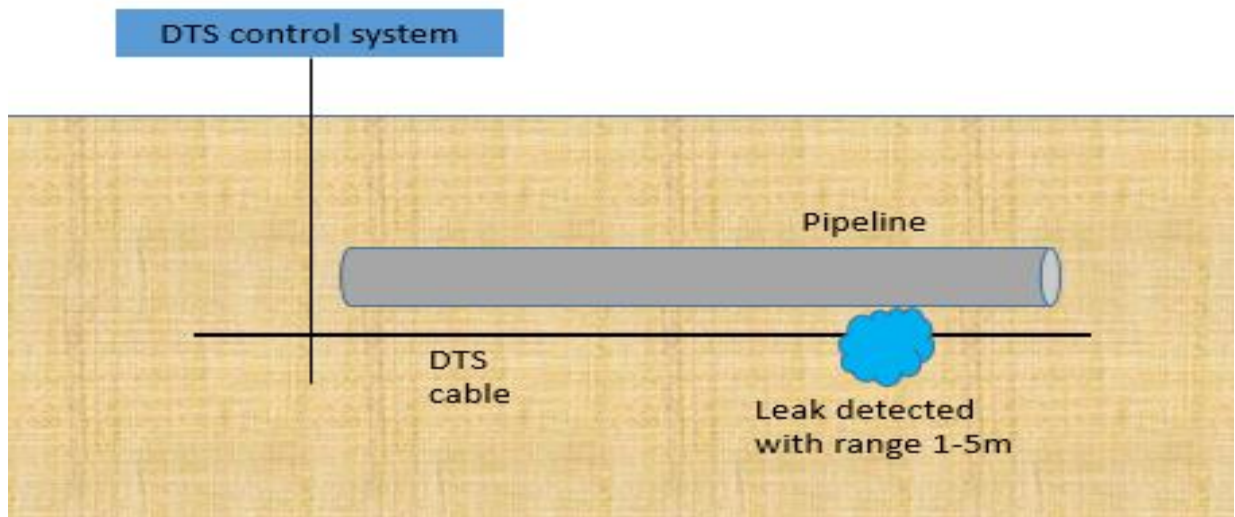


Figure 3.1: Figure showing DTS system for leak detection [37].

### 3.1.2 Real-Time Gas Kick Detection

A combined DTS and DAS system can be used to measure downhole conditions in order to study the velocity of gas migration and water front movement to predict gas kick detection, experiment is applied on a two phase flow(nitrogen-water) in a marine riser where the DTS measures thermal gradients to study movements of gas [6].

### 3.1.3 Monitoring Acid Stimulation Treatments

Acid stimulation job such as the enhancement of formation permeability for naturally fractured reservoirs leads to decrease damages resulting from skin thus enhancing the productivity of the well, where a thermal increase in the formation zone occurs that can be monitored by a DTS system that allows the identification or tracking of the zones where acid injection occurs, thus forming a solution to the uncertainty of the zones receiving the acid [38].

### **3.1.4 Reservoir Geo-Statistical Description**

The utilization of a DTS system provides continuous thermal profile which can be used to estimate robustly the layers petro physical parameters such as porosity and permeability based on the “information theory”, data obtained can be combined with the bottom hole pressure data profile to produce much more reliable results [39].

### **3.1.5 Well Bore Monitoring**

A main application of the DTS system is the thermal measuring of downhole conditions thus providing reservoir temperature with a low cost and efficient technique for both vertical and horizontal wells and giving a continuous profile of temperature along the well allowing many actions to be taken such as remediation of fluid migration behind casing [7].

In steam-assisted gravity drainage observation wells, DTS system with low power was used for thermal monitoring of downhole and shown great performance despite of harsh conditions such as very low temperature [40].

### **3.1.6 Injection and Production Profiling**

DTS system have proven high efficiency for injection profiling for both vertical wells showing continuous real time monitoring of injection profiles that can be analysed by one of the following approaches: stabilized injection-thermal restoration-thermal tracer thus allowing the determination of isolation zones and study the rise of fracture [41], and for horizontal wells providing the thermal signature along the well distance which can lead to the improving of recovery [3].

On the other side, DTS systems are also used for production profiling. For gas wells it is very important to identify the water-breakthrough immediately for operator to take actions by detecting thermal changes, the Joule Thomson effects are the main reason to temperature variation where gas undergoes cooling and water undergoes warming in the production phase due to the pressure decrease [42].

## **3.2 DAS Applications**

Noting that DAS technology is still considered as an immature technology when being compared to DTS, that was implemented more than 20 years ago, but still DAS is invading several sectors of oil field.

### **3.2.1 Multiphase Flow Metering**

DAS offers multiphase flow in pipeline monitoring by providing the speed of sound and vortex speed by analysing the frequency-wavenumber (f-k) plot produced by DAS data, this approach was done on both bubbly and stratified flows, hence showing the flexibility of DAS and ability to determine both flow speed and composition through a non-intrusive multiple zone DAS multiphase flow metering [1]. The analysis of DAS data to obtain both fluid composition and bulk flow rate is done by mono- or bi-dimensional Fourier Transform in order to obtain the speed derivation in a direct method [43]. This application will be discussed in details in the “Sensitivity Study” chapter.

### **3.2.2 Geophysical Applications**

Traditional geophones are starting to be replaced by the DAS systems due to a group of factors including the ability of only one shot record of the whole well given by DAS thus lowering health safety and environmental costs, and the geophones are not permanently installed. DAS also show efficiency in results, where data obtained from both techniques are compatible allowing DAS to be the proper alternative for geophones in cases with high safety risk for long arrays like elongated horizontal wells [44].

An important application of DAS in the geophysics sector is the monitoring of micro-seismic events, with Shell company to be the first to apply DAS technique for micro-seismic events and was set against the geophone datasets, due to the single shot record property of DAS it could be deduced that geophone coverage was bounded compared to full coverage contributing to define the position of these events, but geophones still have higher sensitivity. A perfect example showing comparison between DAS (grey

colour) and Geophone (red colour) is shown in Figure 3.2 where due to the low sensitivity of DAS it was observed that the apex of hyperbola of P-wave disappears. Micro-seismic events are monitored in several DAS channels, by modifying the orientation of these channels DAS events are possible to be positioned in deviated wells. Merging these seismic data with data coming from techniques such as pressure and tracer data it is possible to study or diagnose hydraulic fractures [8].

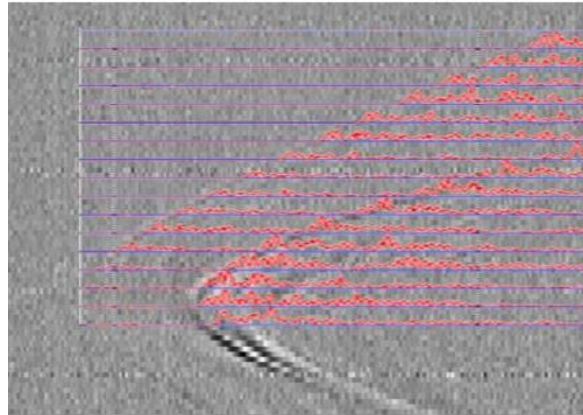


Figure 3.2: Micro-seismic event monitored by Geophone (red colour) and DAS system (grey colour) [8].

### 3.2.3 Hydraulic Fracture Diagnosis

As mentioned before, the employment of DAS usually requires single mode fiber optic cables; an important application of DAS is to monitor hydraulic fractures in tight sand and shale gas reservoirs. The ability of DAS to monitor acoustic events and discriminate between them thus being capable of studying the dynamic behaviour of in-well events using treatment wells of hydraulic fracture represents an important advancement in this field. Using the frequency data obtained, a differentiation between perforation clusters absorbing the fluid and the ones considered during acid injection active [45].

### 3.2.4 Sand Detection

Due to the ability of DAS to monitor several zones simultaneously, it can be utilized to detect the beginning of sand production with the main challenge to identify formation sand from other noise sources thus several experimental studies were done to obtain

the sand production mark, after that a model is obtained. DAS monitoring technique was applied to detect the motion of sand particles by plotting the data versus both time and depth [46].

### **3.2.5 Electric Submersible Pump (ESP) Surveillance**

An intelligent DAS system is designed to inspect or monitor ESP performance due to DAS ability of positioning vibration origins, to understand the performance of ESP Fourier transform must be applied to the variable frequencies generating different harmonics by the pump. Production areas near the pump are affected by the noise produced thus the signals are disrupted and DAS is not able to analyse flow speeds. DAS provides a useful tool for ESP service providers to enhance its effectiveness and optimize its life span [47].

## **3.3 Applications of combined DAS and DTS integration**

### **3.3.1 Gas Lift Surveillance**

DAS and DTS combined system is preferred to be used for gas lift surveillance for onshore and offshore wells on other traditional techniques since it doesn't require any well intervention hence preventing production postponement. DTS provide accurate temperature profiles along wellbore depth. DAS is also used to monitor acoustic events as function of both time and depth, but with one more advantage that is improving signal to noise ratio (SNR) by differentiating between different acoustic events. SNR must be improved due to several reasons such as turbulence associated with the flow and probability of completion crossovers present. DTS and DAS can provide lift-gas injection depth with different approaches and DAS having better resolution.

DTS mechanism to determine the gas-lift depth is simple based on Joule Thomson effect when gases undergo cooling. The DAS mechanism is explained in figure 3.3 as shown below [48].

Frequency bands are formed defining acoustics with less than 1 Hz and more than 1KHz.

To differentiate results, a normalization is applied for frequency on data with noise.

Results versus depth is provided to provide injection depth.

Active gas lift is identified in case of acoustic power is clear for both bands.

Figure 3.3: Flow chart of DAS data analysis mechanism [48].

### 3.3.2 Fluid Ingress Position Identification

The utilization of both DAS and DTS for identifying production zones of fluid like water breakthrough needs couple of fiber optic cables which is easy since multiple optical fiber are present in a mono-control line. Property of DAS in determining energy consumption and DTS in temperature tracing and thermal models provides necessary information to investigate water ingress. Increasing certainty for DTS results require more monitoring duration intervals thus forming a rigorous study of thermal variations from transient state to equilibrium state especially in case of perturbations in well. Experiments were performed to study the effect of Electric Submersible Pump (ESP) present in the hole due to the noise produced when it operates, where no observation of a shift for production intervals in case of active or inactive ESP, but the production areas near the ESP were characterized by less clear signal due to the noise created from the pump [49].

## 3.4 Applications of DPS

### 3.4.1 Production Data Analysis

DPS system is utilized for collecting pressure data in real time, where this pressure sensor is positioned at every cluster of hydraulic fracture to get a continuous pressure profile. To analyse the pressure data obtained a tri linear model is developed, this model describes a horizontal well with five hydraulic fractures described by different half-lengths for an unconventional shale reservoir. Hence the pressure data will provide the effect or bid rate of every hydraulic fracture cluster in the production process. A plot of the contribution ratio as a percentage versus the hydraulic fracture half-lengths is provided to understand the proportionality between the results of the analytical model to the half-lengths as shown in figure 3.4 [50].

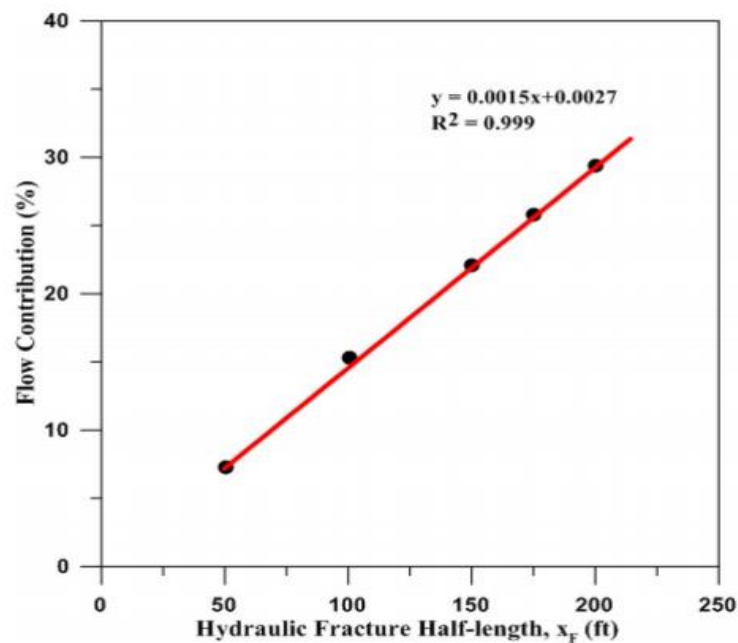


Figure 3.4: Plot showing flow contribution versus Hydraulic fracture half-length [50].

### 3.4.2 Near Wellbore Permeability Estimation for Horizontal Well

DPS system is a powerful tool that contributes in the estimation of specific productivity index, near well bore permeability, or inflow profiles. This technique is preferred due to the big pressure drops occurring in production intervals of horizontal wells. The DPS is positioned beyond the casing to provide the sand face pressure which makes it clear for surrounding-well reservoir flow. Thus providing continuous real time pressure profile which will be analysed with the inversion method applied to the numerical model to obtain productivity index. Further experiments were applied to understand the effect of the increasing noise which is summarized in the following figure 3.5 [51].

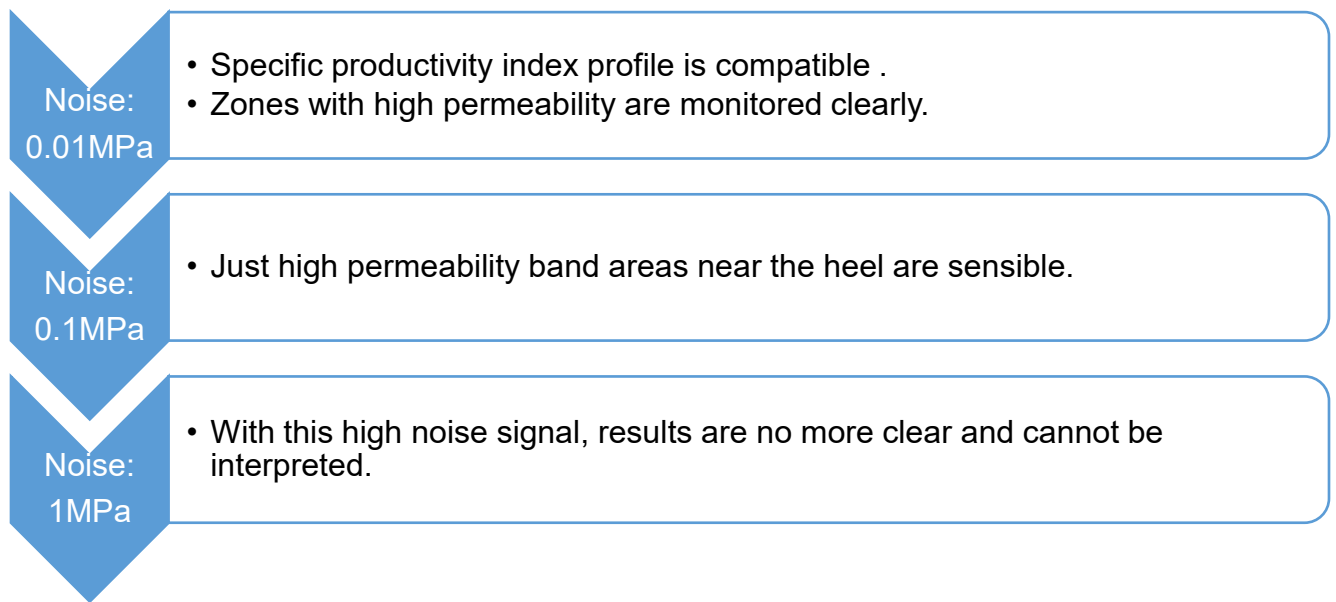


Figure 3.5: Flow chart showing effects of increasing noise level [51].

# Chapter 4: Literature Review

A literature review is done to encompass scientific papers and articles that studied the multiphase flow characterisation or metering using different fiber optic sensing configurations. These include several techniques to study the multiphase flow including Experimental, Modelling, and using Computational Fluid Dynamics (CFD). Thus for each of the mentioned techniques a unique section is provided. The purpose of the review is to organise the conditions and mechanisms already tested, hence highlighting research gap in previous studies.

## 4.1 Experimental Papers

In this part of literature review, some experimental papers using DFOS technique are tested for multiphase flow metering for both horizontal and vertical pipes and being compared with flow regime maps from literature.

The following table shows four experiments done by fiber optic sensing, showing all experiment conditions such as fluids used and their properties when mentioned, thermodynamic properties of the system, the orientation of the pipe, a bullet point summary of the main findings, and finally the research gap that can be extracted from the experiment.

Table 4.1: Experiments using DFOS for multiphase flow metering.

Author (Year)	Experimental Technique	Fluids	Pipe Dia, cm (inch)	Liquid Flow rate	Flow Velocity	Orientation	Main findings	Research Gap
Feo et al. (2019)	Distributed fibre optic sensing (DTS-DAS)	Gas (Nitrogen), Liquid (water).	-	Water: 0.636 m <sup>3</sup> /min	Water: 1.615 m/s (5.3ft/s)	Vertical	<p>-DTS and DAS technologies are valid for early kick detection and monitoring two phase flow behaviour in offshore facilities.</p> <p>-DTS allow both temperature and temperature gradients measurement, and DAS allow gas and water front to be monitored.</p>	<p>-Substitution of water with non-Newtonian fluid scaling real multiphase flow in drilling operation.</p>

<p>Ruixi et al., (2013)</p>	<p>Infrared ray and Laser optical technology</p>	<p>Gas(air). Liquid (water). Solid (pig particles) made from metal and rubber for pig detection.</p>	<p>5 cm (1.968 inch)</p>	<p>-</p>	<p>Air: 0.1-8 m/s (0.328-26.25 ft/s)  Water: 0.05-1.1m/s (0.164-3.61 ft/s)</p>	<p>Horizontal</p>	<p>-Detection of liquid slug and pig for horizontal pipelines.  -Different flow patterns including bubble, slug, stratified, and wavy can be identified by analysis of output signal.  -Identification of pigging slug in pigging operations using both laser and infrared ray.</p>	<p>-Application on bigger pipe diameter to identify flow regimes using Probability Density Function curves.  -Extending the experiment for three phase oil-water-gas flow.  -Extending the experiment for an inclined pipe to study effect of inclination on results.</p>
<p>Baroncini et al. (2015)</p>	<p>Optical Fiber Bragg Grating (FBG)</p>	<p>Gas(air). Liquid (water). No solid particles</p>	<p>-</p>	<p>-</p>	<p>Air: 0-2.5 m/s (0- 8.2 ft/s)  Water: 0-2.5 m/s (0- 8.2 ft/s)</p>	<p>Horizontal</p>	<p>-Monitoring the strain produced by flowing fluid over optical fibers.  -Optical FBG are applicable for bubble or slug flow regime condition in pipelines.  -Optical FBG can be used to determine mass flow rate of one phase flow.</p>	<p>-Studying the effect of diameter size effect on flow patterns.  -Stating the viscosity of the fluids used.</p>

Finfer et al. (2015)	Non-Intrusive Distributed Acoustic Sensing (DAS)	Gas, Liquid(oil). No solid particles	6.89 cm (2.71 inch)	Gas: 0-0.0277 m3/min Oil: 0.27-0.564 m3/min	Gas: 0-0.12m/s (0-0.394 ft/s) Oil: 1.21-2.52m/s (3.97-8.268-ft/s)	Horizontal	-The employment of sound speed to attain flow speed and gas holdup respectively in bubbly flow. -In case of stratified flow, vortex tracking must be used to attain flow velocity of each fluid phase.	-Capability of applying DAS to a three phase system.  -Monitoring sound speed variation on a long duration (weeks-months) in field practice to allow reservoir monitoring.
----------------------	--	--------------------------------------	---------------------	--	--	------------	---	--

## 4.2 Modeling Papers

This section summarizes papers done using modeling techniques for multiphase flow regime identification or metering, mainly using wavelet transform and probability density function techniques.

Table 4.2: Summary of Modelling DFOS for multiphase flow metering.

Author (Year)	Experimental Technique	Fluids	Pipe Dia, cm (inch)	Liquid Flow rate	Flow Velocity	Orientation	Main findings	Research Gap
Fidaner et al.,(2017)	Distributed Acoustic Sensing analysis with Wavelet Transform.	Oil, Gas	-	-	-	-	<p>-A forward model is used to realte DAS multiphase flow through a set of analytical relations.</p> <p>-Wavelet transform is applied in the inverse model to estimate multiphase flow rate.</p> <p>-Combining wavelet transform results with neural network can provide also flow regimes of multiphase flow.</p>	- The ability of applying the technique used to three phase flow system in pipelines (solid-liquid-gas or liquid-liquid-gas).
Fordham et al., (1999)	Local Fiber optic sensors	Gas(air), Liquid (water and kerosene)	7.8cm (3.07 inch)	-	<p>Superficial:</p> <p>Oil: 0.308m/s (1.01 ft/s)</p> <p>Water: 0.314 m/s (1.03ft/s)</p>	-	<p>-Local probe method facilitates the identification of flow regimes in inclined pipelines.</p> <p>-Cleaved and Corner-sensors are applied to three phase system in both bubbly and low gas fraction cases.</p>	-

Author (Year)	Experimental Technique	Fluids	Fluid condition / T and P	Flow Velocity And Pipe Diameter	Orientation	Main findings	Research Gap
Chakrabarti et al., (2006)	Wavelet multi resolution technique and Probability Density Function (PDF) analysis	Liquid: Water and kerosene	<p>Viscosity: Water (0.84 cp) and Kerosene (1.2 cp)</p> <p>Interfacial tension: 0.045 N/m</p> <p>Density Kerosene (787 kg/m<sup>3</sup>) and Water (1000 kg/m<sup>3</sup>)</p> <p>/</p> <p><b>Pressure:</b> 101.325 Kpa (14.69 psi)</p> <p><b>Temp:</b> 24.85 °C (76.73 F)</p>	<p>Superficial: Kerosene: 0.03-1.5 m/s (0.098-4.92 ft/s)</p> <p>Water: 0.03-1.5 m/s (0.098-4.92 ft/s)</p> <p>/</p> <p>Diameter: 2.54cm (1inch)</p>	Horizontal	<p>-Current non-intrusive optical technique surpass limitations like oil sticking to probe surface present in intrusive, and gives immediate response with inexpensive cost.</p> <p>-Probability Density Function analysis and Wavelet Transform allows recognition of discrete structures describing distinct flow regimes, building a flow regimes map.</p> <p>-The obtained map complies with previous literature outcomes showing effectiveness.</p>	<p>-The success of this technique on two different phases.</p> <p>-Usage of more viscous liquids to study effect of viscosity on results.</p>

### 4.3 CFD Papers

This final section discuss papers done on multiphase flow using computational fluid dynamics software for numerical simulation for both single and multiphase flow profiling.

Table 4.3: CFD papers using DFOS for multiphase flow metering.

Author (Year)	Experimental Technique	Fluids	Fluid Properties	Pipe Dia, cm (inch)	Orientation	Main findings	Research Gap
Ouyang et al., (2004)	TIPP simulation program	Gas, Liquid(Oil-Water)	Oil-Water interfacial tension: 0.03N/m Oil-Gas interfacial tension: 0.06N/m Oil API=40 Specific Gas gravity=0.7	-	Horizontal, Vertical, Deviated	-Parametric study(deviation-Joule Thomson effect-fluid phase) applied to understand effect on forward model.  -Using Distributed Temperature Sensing allows flow profiling for one-phase flow, and multi phase flow in case of obtaining extra data like well-bore pressure profile.	-Parametric study on the effect of high viscous fluids on temperature profile.
Kortukov et al. (2019)	Numerical Simulation Software	Gas(Air) Liquid (Water and/or Oil)	-	-	Horizontal Well	-Application of Pressure Temperature Rate-transient Analysis (PTRA) through producing variable rates causing thermal change, the fiber optic installation is capable of simulating the production inflow phase content( single or multiphase flow).	-Studying the validity of such numerical model to deviated wells.

Author (Year)	Modelling Technique	Exp Conditions	Pipe Dia, cm (inch)	Orientation	Main findings	Research Gap
Shirdel et al., (2019)	Numerical simulation	-	8.89cm (3.5 inch)	Horizontal	<p>-A work-flow is done to simulate steam injection flow to understand variant flow regimes in horizontal wells.</p> <p>-Enhancing steam conformance due to high efficiency of this monitoring technique comparing with traditional ones.</p> <p>-Clustering optimization techniques are used to combine several algorithms for flow profiling to get better final flow profile.</p>	-Applying this methodology for higher fiber optic data sets (tera bytes).
Espiner et al. (2014)	Numerical Simulation	Gas, Liquid, Solid (Pig particles)	50.8cm (20 inch) And 30.48cm (12 inch)	-	<p>-Leak detection can be done either by detection of temperature changes around leakage space, or by Distributed Vibration Sensing according to real time data to monitor vibrations along whole distance of pipe.</p> <p>-CFD is used to simulate gas flow from leakage.</p> <p>- Distributed Vibration Sensing can be used to monitor the motion of the pipeline pigs.</p>	-

# Chapter 5: Sensitivity Study on Phase Fraction

This chapter is divided into three sections, principle of operation of Distributed Acoustic Sensing (DAS) in measuring Speed of Sound (SoS) will be explained in the first section, while the second demonstrates how can we use SoS in multiphase flow metering, and finally the third section will include sensitivity study performed on several parameters to understand their effects.

## 5.1 SoS determination using DAS

The advantage of “distributed sensing” of fiber optics generally and DAS in particular can be used in order to obtain a continuous profile of the acoustic field along the entire length of the pipe.

Determination of SoS in multiphase flow follows using DAS technology is explained in details according to the following procedure:

- a) DAS fiber optic cable is placed side by side with the pipe. Note that in some cases, usually for laboratory scale, fiber cable can be wrapped helically around the pipe. Acoustic field is present in all production/transportation zones.

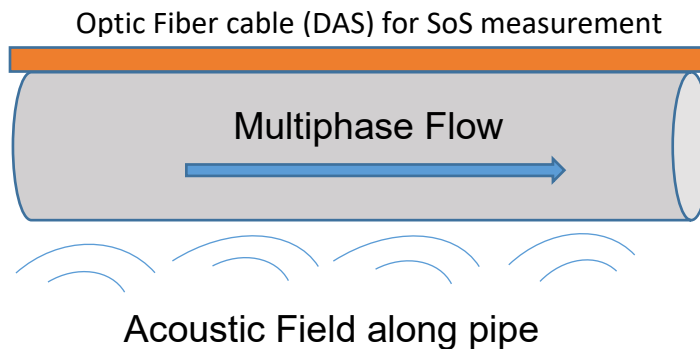


Figure 5.1: Acoustic field along total length of pipe.

- b) Sound waves have the ability to propagate in both directions, co-current and anti-current flows. Thus two waveguides with opposite directions are observed as shown in figure 5.2.

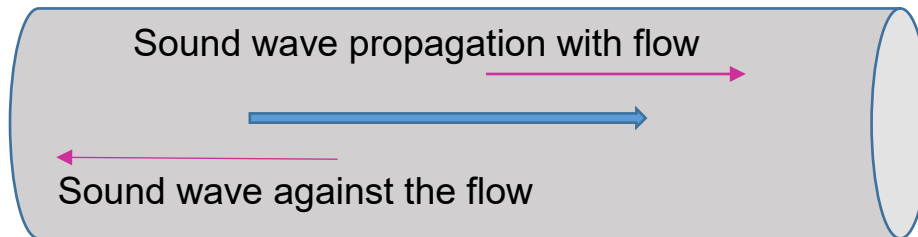


Figure 5.2: Sound waves in opposite directions of flow.

- c) Acoustic waves produce pressure variations in the fiber that can be translated into refractive index perturbations along the pipe. Hence a backscattering phenomenon of a portion of light described by Rayleigh scattering as explained in **section 2.2.2** is observed.



Figure 5.3: Backscattered signal due to acoustic field effects.

- d) Both phase and amplitude of the backscattered optical signal can be measured by the DAS configuration giving the continuous profile depending on the coherent OTDR. Thus phase fluctuations enable DAS to provide the time-length or time-depth plot along the pipe or wellbore.

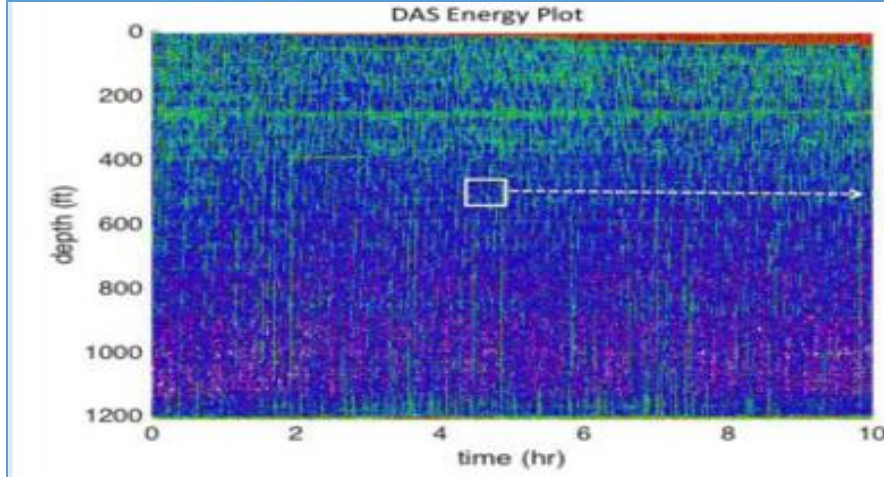


Figure 5.4: Depth-Time curve from DAS data [4].

- e) A two dimensional Fourier transform is applied to the time-length (t-d) space to convert it to frequency-wavenumber (f-k) space as shown in figure 5.5. Signal analysis of noise in the new space shows two lines (one representing the co-current speed wave and the other representing anti-current speed wave), where the SoS can be determined from the slope of the lines.

The equation relating speed of sound to frequency  $f$  and wavelength  $\lambda$  is given by:

$$SoS = f * \lambda \quad (5.1)$$

Where wavenumber is defined by  $k=2\pi/\lambda$ , thus the final equation showing how SoS can be determined from the slope of the line is:

$$f = \left(\frac{SoS}{2\pi}\right) * k \quad (5.2)$$

Where  $f$  is the frequency measured in Hz, SoS in m/s, and  $k$  is wavenumber measured in  $m^{-1}$ .

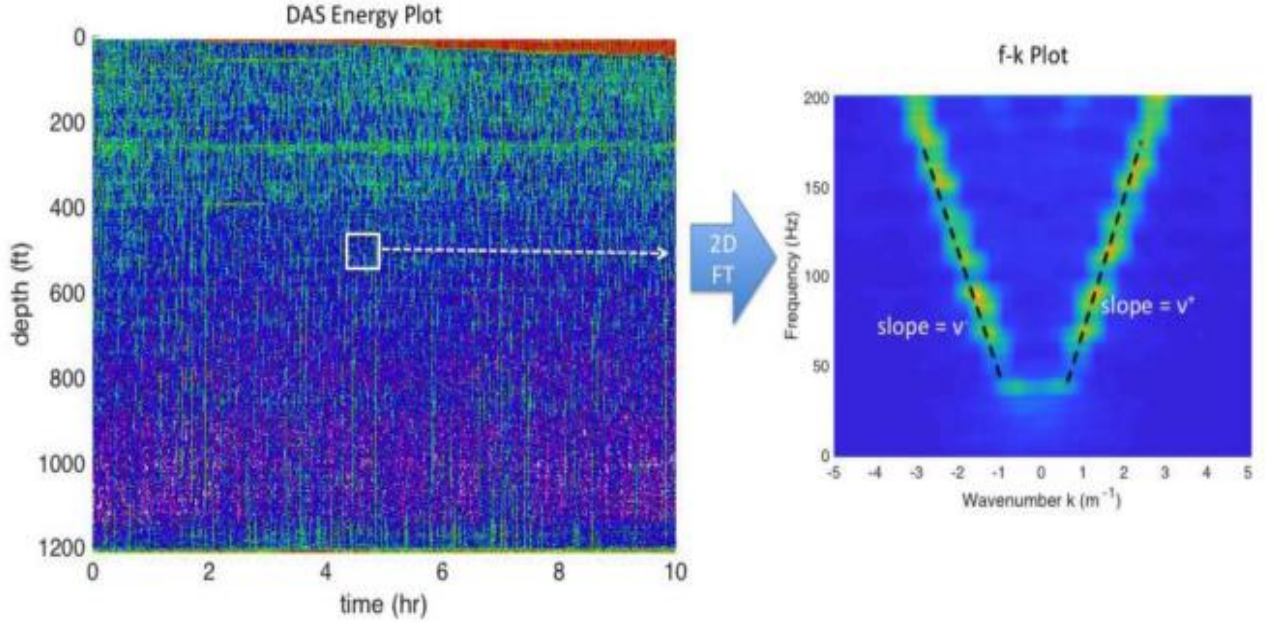


Figure 5.5: 2D Fourier transform of DAS data [4].

As mentioned that two different values of SoS are obtained from the f-k space, they can be noted as **SoS<sup>+</sup>** and **SoS<sup>-</sup>**, according to the Doppler shift concept applied to both velocities we can define each value by:

$$SoS^+ = SoS + V \quad (5.3)$$

$$SoS^- = -SoS + V \quad (5.4)$$

Where SoS is the true speed of sound of the flow medium, V is the flow speed based on SoS measurement. Hence we can deduce formula of V (Equation 5.5) by adding equations 5.3 and 5.4, and formula of SoS (Equation 5.6) by subtracting equation 5.4 from equation 5.3 to get:

$$V = \frac{SoS^+ + SoS^-}{2} \quad (5.5)$$

$$SoS = \frac{SoS^+ - SoS^-}{2} \quad (5.6)$$

## **5.2 Utilization of SoS for multiphase flow metering**

As mentioned in the previous section, SoS continuous profile along length of the pipe can be obtained from DAS. For the next step, SoS is implemented in a procedure for multiphase flow metering. Three different sections will be discussed depending on the nature and number of flows. SoS provides the total solution to the multiphase flow metering in some cases, and in more complex cases SoS presents the major part of the solution with the requirement of additional information. Determination of SoS shown in previous section is the same for both single and multiphase flows. Hence using the two keys (flow velocity and phase fraction) obtained from DAS, multiphase flow metering can be done.

### **5.2.1 Case of single phase flow metering**

Note that SoS can be also used in single phase flow such as in the cases of monitoring injector profiles [2]. The understanding of single phase is essential since in special cases of multiphase flow such as above bubble point for oil flows, the DAS configuration deals with it as a single phase flow. Usually for downhole monitoring applications this case is observed.

### **5.2.2 Case of two phase flow metering**

When the multiphase flow is a bi-flow, we are interested mostly in liquid-liquid flow such as oil-water flow and liquid-gas flow such as oil-gas flow. Both cases are very different and so the solution is. Mainly the difference is due to the big contrast in densities between both cases, where the density parameter is a major factor in the correlation used for both cases between SoS and phase fraction  $\phi$ . The majority of experimental papers testing the efficiency of DAS in two phase flow metering refer to the same correlation that was developed in 1941 finding the relation between SoS and phase fraction  $\phi$  [52]. In recent years, more papers are published under the section of DAS assessment in multiphase flow (two phase flow) metering [1] [2], and were based on the

same correlation for SoS that was based on a very important assumption that provides the multiphase flow is in a turbulent condition ensuring that the two fluids are well mixed, otherwise in case of stratified flows or laminar conditions the following equation is not valid since we need to introduce some correction factors. The correlation between SoS and  $\phi$  in well mixed flow is given by equation 5.7:

$$(SoS)_m = \frac{1}{\sqrt{[(1 - \phi)\rho_1 + \phi\rho_2]\left[\frac{1 - \phi}{\rho_1 a_1^2} + \frac{\phi}{\rho_2 a_2^2}\right]}} \quad (5.7)$$

Where  $(SoS)_m$  is the speed of sound in the mixture,  $\phi$  is the phase fraction,  $\rho$  and  $a$  are the density and speed of sound of individual phases respectively.

Equation 5.7 is a quadratic equation for  $\phi$ , if being developed we can have the following quadratic equation for phase fraction:

$$A\phi^2 + B\phi + C = 0 \quad (5.8)$$

Where A,B, and C are given by the following expressions:

$$A = \frac{1}{a_1^2} + \frac{1}{a_2^2} - \frac{\rho_1}{\rho_2 a_2^2} - \frac{\rho_2}{\rho_1 a_1^2} \quad (5.9)$$

$$B = \frac{\rho_1}{\rho_2 a_2^2} + \frac{\rho_2}{\rho_1 a_1^2} - \frac{2}{a_1^2} \quad (5.10)$$

$$C = \frac{1}{a_1^2} - \frac{1}{(SoS)_m^2} \quad (5.11)$$

Thus we expect two roots from the equation 5.8,  $\phi_1$  and  $\phi_2$  given by  $0 < \phi_1 < \phi_2 < 1$ . In the following section we will discuss the uniqueness of the solution relating it to the physical meaning and conditions of the flow.

Note that DAS provides both keys to characterize two phase flow, the first is SoS that leads to  $\emptyset$  as it will be discussed in the next page and volumetric flow rate that can be calculated from equation 5.12:

$$Q = V * A \quad (5.12)$$

Where Q is the volumetric flow rate, V is the speed of flow obtained from Doppler shift, A is the cross-sectional area of the pipe.

### 5.2.2.1 Liquid-Liquid Flow

In the case of liquid/liquid flow, resolving the multiphase flow is an easy task, since a typical flow where we have both oil and water fluids shows that there is a unique solution as shown in figure 5.6 for the phase fraction  $\emptyset$  which is in this case equal to Water in Liquid Ratio WLR. Mathematically speaking, the only accepted root of the equation 5.8 is  $\emptyset_2$ , since  $\emptyset_1$  gives negative value which is impossible for phase fraction or gives a value higher than 1 which is also rejected.

The trend of the curve is increasing for higher values of WLR, since for high values of WLR the mixture behaves more like water, where SoS in water is higher than SoS in oil so  $(SoS)_m$  gradually increases with increasing WLR.

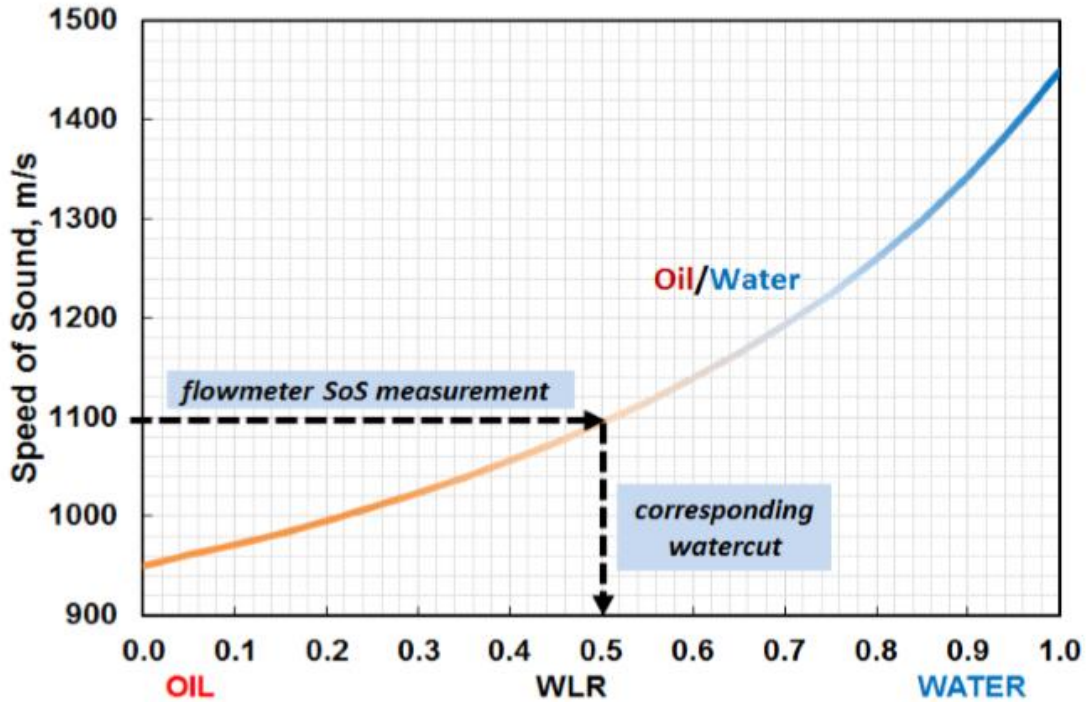


Figure 5.6: Typical SoS curve function of WLR in Oil/Water flow [2].

After the determination of WLR, the process of multiphase flow characterization in order to understand the flow patterns can be continued by calculating the flow rates of each phase by the following equations:

$$Q_o = (1 - WLR) * Q_t = (1 - WLR) * V * A \quad (5.13)$$

$$Q_w = WLR * Q_t = WLR * V * A \quad (5.14)$$

Where  $Q_o$ ,  $Q_w$ , and  $Q_t$  represent the oil, water, and total flow rates respectively.  $V$  is the flow velocity, and  $A$  is the cross-sectional area.

### 5.2.2.2 Liquid-Gas Flow

A liquid-gas flow is more complex than liquid-liquid flow; this is due to the fact that this type of flows exhibit a dual solution for phase fraction  $\phi$  which is equal in this case to the Liquid Holdup HL. Typical curve of such flow is the Oil-Gas flow as shown in figure 5.7, which shows that the measurement of SoS provide a dual solution, with the real

value can be determined by classifying the production or transportation zone either oil-rich ( $\phi_2$  is the solution since  $\phi_2 > \phi_1$ ) or gas-rich ( $\phi_1$  is the solution since  $\phi_1 < \phi_2$ ).

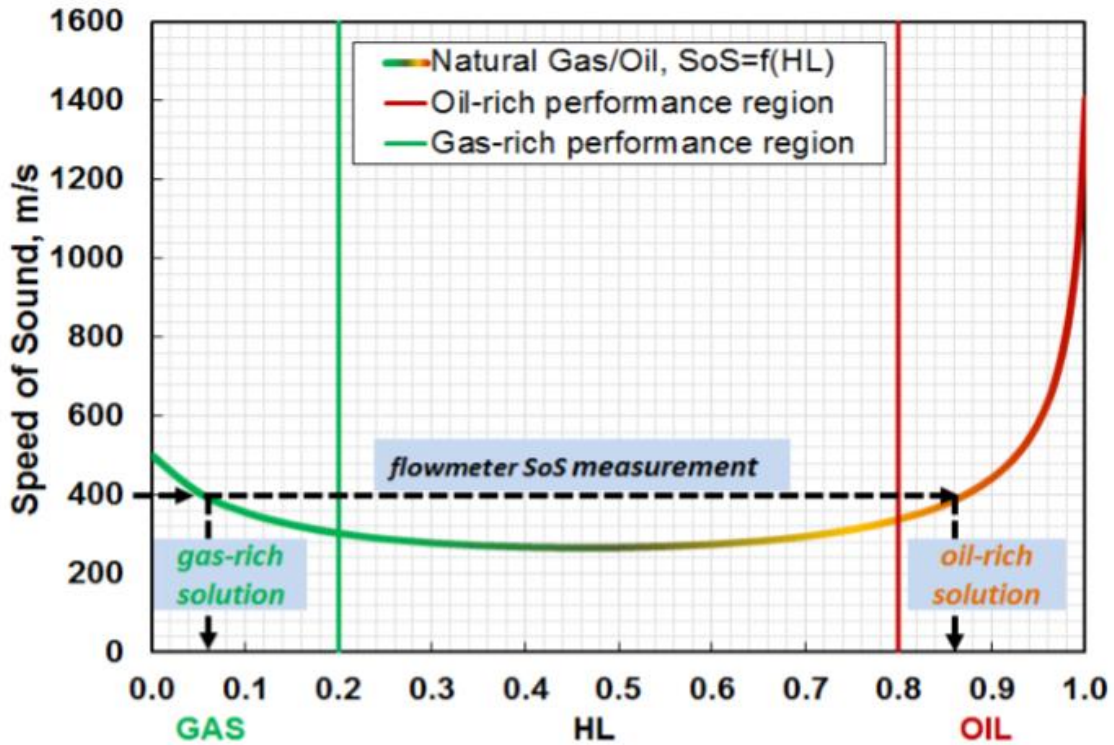


Figure 5.7: Typical SoS curve function of HL in Oil/Gas flow [2].

As HL increases to 0.5,  $(SoS)_m$  decreases, for more increase in HL it is observed that the trend starts to become increasing, for high values of HL greater than 0.8 a very sharp increase occurs in  $(SoS)_m$ .

From another point of view a sharp decrease in the curve for high HL values could help in downhole monitoring applications such as gas breakthrough for oil production wells.

### 5.2.3 Case of three phase flow metering

In three phase flow the SoS of the mixture represents a major part of the solution resolving multiphase flow but not the complete one, since in this case the plot or data referring to is SoS function of density of the mixture, where both Water in Liquid Ratio WLR and Liquid Holdup HL contours are present in the curve as shown in figure 5.8.

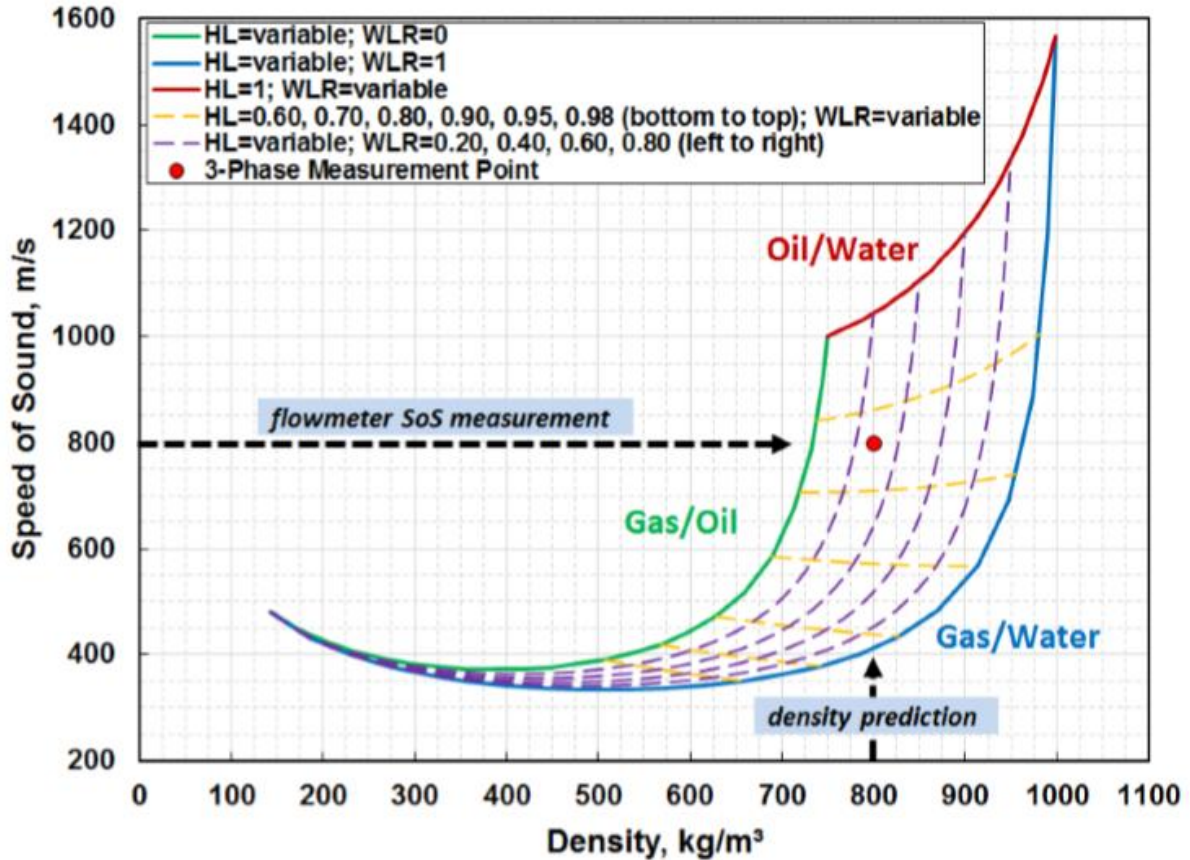


Figure 5.8: Typical SoS curve function of Mixture Density in Water/Oil/Gas flow [2].

The procedure requires additional information other than SoS of the mixture, that is in this case the density of mixture  $\rho_m$ . Other parameters can be measured with SoS to resolve the three phase flow.

The first step in this case as in figure 5.9 is the density mixture determination, which follows an iterative procedure after measuring the differential pressure along the pipe as shown in figure 5.9.

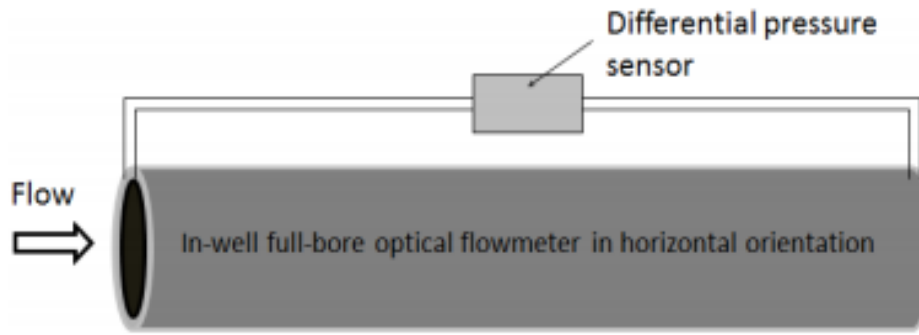


Figure 5.9: Differential pressure sensor configuration [5].

Measurement of differential pressure allows the determination of  $\rho_m$  through an iterative method described in details [5], with the procedure based on equation 5.15:

$$\rho_m = \frac{\Delta P}{\frac{1}{2} v^2 f \frac{L}{D}} \quad (5.15)$$

Where  $\rho_m$  is the mixture density,  $v$  is the flow velocity,  $f$  is the friction factor which is function of the Reynold Number,  $L$  is the length of the interval of pipe,  $D$  is the diameter of the pipe.

Back to figure 5.8, using the pair SoS and  $\rho_m$  we can obtain a unique pair solution (WLR,HL), thus all phase fractions can be determined and then flow rates of individual phases ( $Q_g, Q_w, Q_o$ ) of gas/water/oil respectively according to the following equations:

$$Q_g = (1 - HL) * V * A \quad (5.16)$$

$$Q_w = HL * WLR * V * A \quad (5.17)$$

$$Q_o = HL * (1 - WLR) * V * A \quad (5.18)$$

Where  $A$  is the cross-section area and  $V$  is the flow speed.

### 5.3 Sensitivity study on phase fraction of two phase flow

Sensitivity study can be described as a critical tool used to understand the behaviour or sensitivity of a dependent variable when other independent variables are increased or

decreased in a mathematical model simulating a specified concept.

In this section the results of sensitivity applied on several parameters will be demonstrated and discussed. The sensitivity study is applied on equation 5.7 with some deformations to present how equation becomes of phase fraction of two phase flow. However a correction is applied to the equation to relate the bulk value of speed of sound in the fluid mixture  $(SoS)_m$  to the speed of sound on tubing that is in reality the measured parameter taking into account the physical properties of the pipe including diameter, thickness, and Young modulus of elasticity of the pipe material. Ignoring this correction might lead to misleading values of phase fraction and flow rates, since our purpose is to use DAS for multiphase flow metering, and DAS measures the SoS on the pipe not the bulk value in the mixture. The corrected parameter will be noted as  $(SoS)_p$  given by equation 5.19 [4].

$$(SoS)_p = \frac{(SoS)_m}{\sqrt{1 + \frac{d * \rho_m * (SoS)_m^2}{E * h}}} \quad (5.19)$$

Where  $d$  is the pipe diameter,  $\rho_m$  is the mixture density,  $E$  is the Young's modulus of elasticity of the pipe material,  $h$  is the pipe wall thickness.

By developing the equation 5.19 as done previously in equation 5.8 we obtain a new quadratic equation for the phase fraction with its coefficients (A' B' C') as shown in equations [5.20-5.23].

$$A'\phi^2 + B'\phi + C' = 0 \quad (5.20)$$

$$A' = \rho_2 - \rho_1 \quad (5.21)$$

$$B' = \rho_1 \quad (5.22)$$

$$C' = \frac{\frac{1}{(SoS)_p^2}}{\frac{1}{\rho_1 a_1^2} - \frac{1}{\rho_2 a_2^2} - \frac{d}{E * h}} \quad (5.23)$$

Note that the formula of speed of sound  $a$  for fluids is given by equation 5.24:

$$a = \sqrt{\frac{B}{\rho}} \quad (5.24)$$

Where  $B$  is the bulk modulus, and  $\rho$  is the density.

### 5.3.1 Case of Liquid-Liquid flow

Considering a Water-Oil flow, phase fraction is Water in Liquid ratio defined by:

$$\phi = WLR = \frac{V_w}{V_w + V_o} \quad (5.25)$$

Where  $V_w$  is the volume of water and  $V_o$  is the volume of oil. Six parameters are chosen for the sensitivity study which are the oil density, bulk modulus, temperature, pipe diameter, pipe wall thickness, and pipe Young's modulus of elasticity. A discussion is present for most of the plots to explain the trend.

The study of WLR is essential for flow regime identification, since the variation of WLR affects the flow regime map. This is related to the fact that for low values of WLR, dispersion of water in oil faces no obstacles, while for high values of WLR the separation between phases due to the coalescing of water droplets occurs [53].

#### 5.3.1.1 Oil density effect

Oil density parameter is also related to oil speed of sound, since its variation also affects the speed of sound as shown in equation 5.24. Range of oil density was between [720-980] Kg/m<sup>3</sup>, to take into account different classifications of crude oil from light to heavy oil. The following curve shows the phase fraction variation function of SoS for different oil density values.

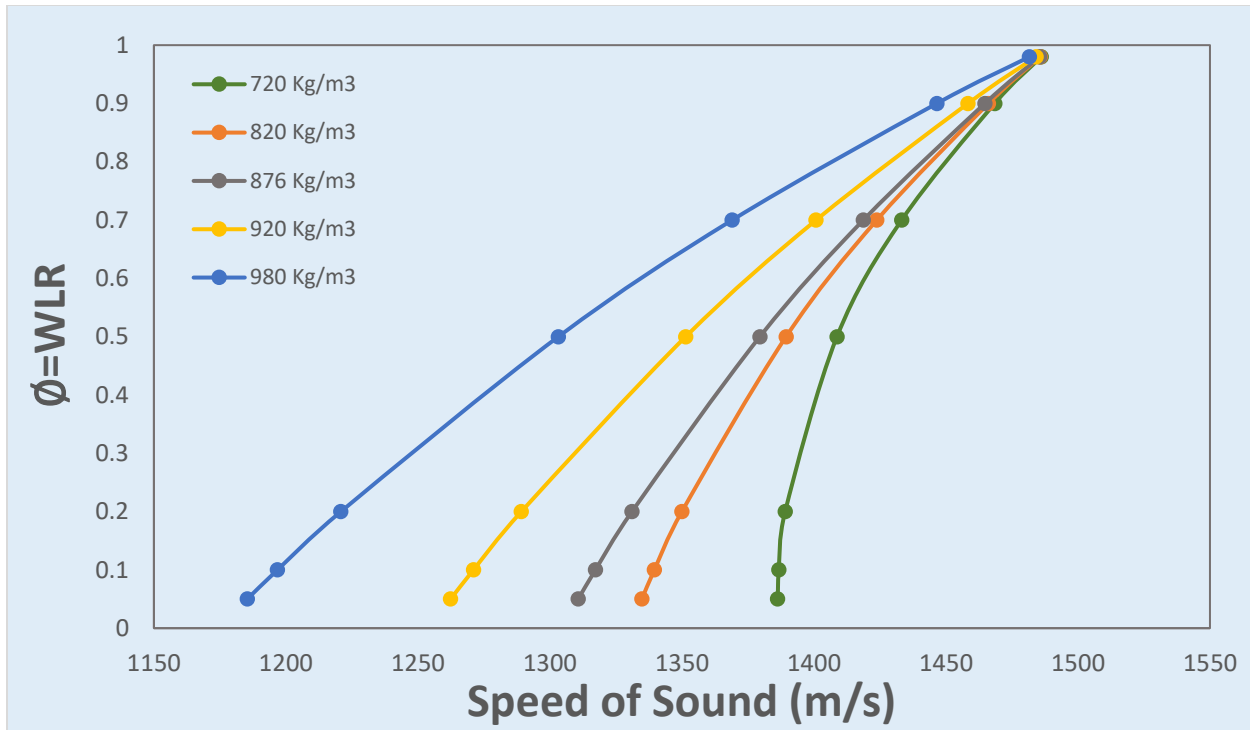


Figure 5.10: Oil density effect on WLR curve versus SoS.

**Trend:**

As the oil density  $\rho_o$  increase, the WLR increase.

**Discussion:**

As the density of the oil phase increase, the volume of oil will decrease since they are inversly proportional to each other. Volume of water will increase leading to increase in the WLR.

For values of WLR greater than 0.9, the sensitivity to oil density decrease significantly since the mixture now behaves similarly to water (composing more than 90% of the mixture) where we observe the SoS detected on the pipe  $\sim 1480$  m/s which is the SoS in water.

**5.3.1.2 Oil Bulk Modulus effect**

The bulk modulus of crude oils or petroleum usually varies in the range of [1.05-1.49] GPa which will be considered for this parameter. The following curve shows the Phase fraction variation function of SoS for different oil Bulk Modulus values.

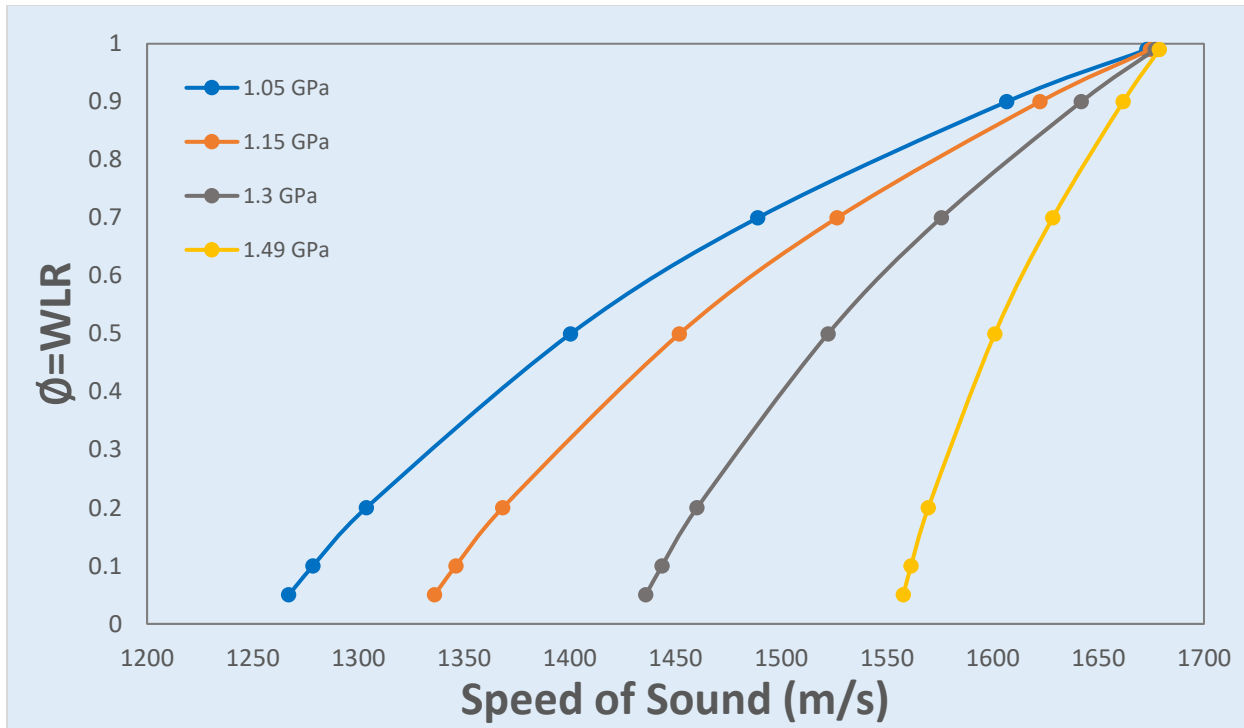


Figure 5.11: Oil Bulk Modulus effect on WLR curve versus SoS.

**Trend:**

Water Holdup WLR increase with the decrease of Bulk Modulus of oil  $B_o$ .

**Discussion:**

The bulk modulus of a fluid can be defined as the measure of resistance to compression, the following equation shows the formula of  $B$  :

$$B = -V \frac{\Delta P}{\Delta V} \quad (5.26)$$

Where  $V$  is the volume,  $\Delta V$  and  $\Delta P$  are the change in volume and pressure respectively. By modifying this equation, we can deduce that for a specified pressure drop of the fluid, the change in volume of oil will be “less” in case of higher bulk modulus of oil, thus obtaining a higher phase volume of oil than in case of higher bulk modulus.

Noting that water has a constant specified bulk modulus (2.1 GPa), according to equation 5.25 the oil volume is in the denominator, and it increases with  $B_o$  increase. Hence WLR will increase as  $B_o$  decreases.

### 5.3.1.3 Pipe diameter effect

The pipe diameter effect was studied after varying values from laboratory scale to field or industrial scale, a range including [0.11-1] m. The following plot shows the WLR variation function of SoS to show diameter effect.

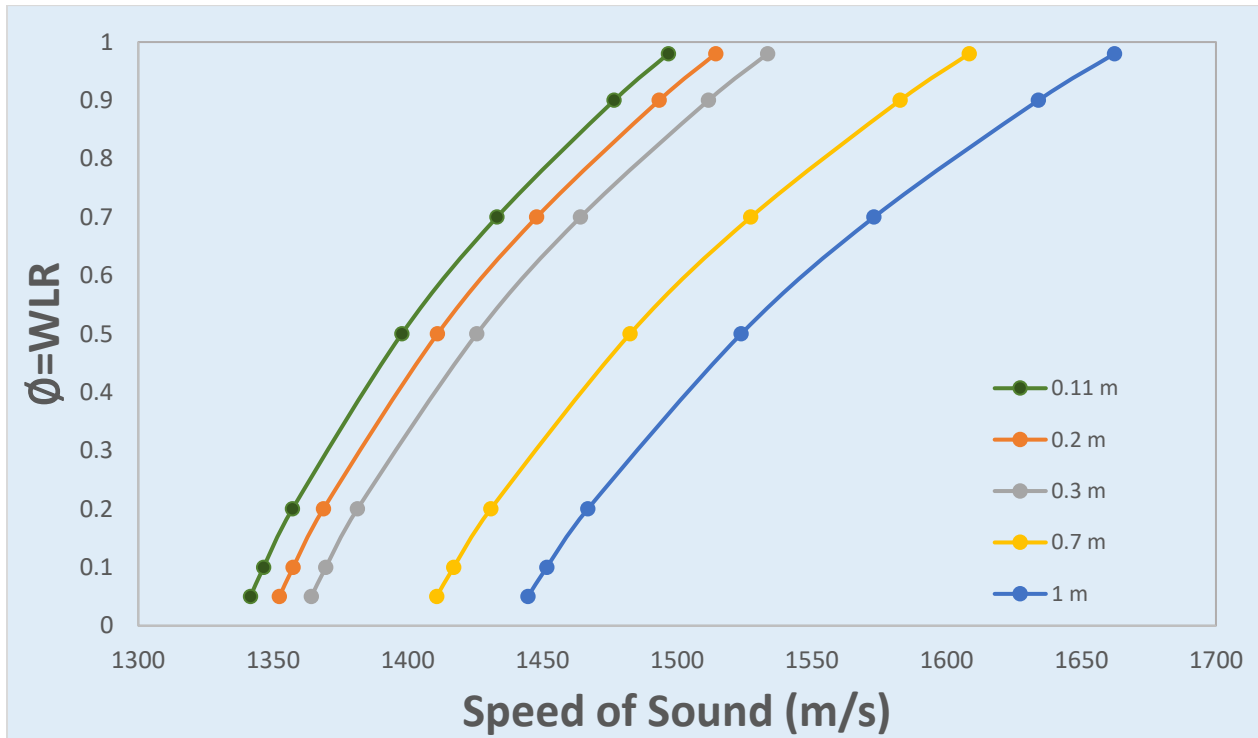


Figure 5.12: Pipe diameter effect on WLR curve versus SoS.

#### **Trend:**

As the diameter of the pipe increase, the Water in Liquid ratio WLR decreases.

#### **Discussion:**

We can deduce an inversely proportional relation between WLR and pipe diameter. The increase in the diameter of the pipe increases the cross-sectional area through which the fluids will flow, which will lead to decrease in the superficial velocities of both water and oil. According to flow regime maps of water-oil two phase flow, the multiphase mixture at high oil and gas superficial velocities is Dispersed oil in water (o/w) flow as shown in figure 5.13-A due to emulsion effects, reduction of velocity of

both fluids produces a Stratified flow regime as shown in figure 5.13-B, where the oil appears no more as dispersed phase but as a continuous phase separated from water at the bottom. Hence the oil phase volume " $V_o$ " increases while the water phase volume " $V_w$ " decreases, resulting in a decrease in WLR.

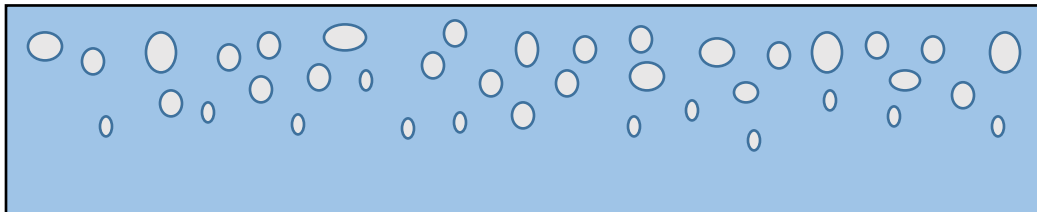


Figure 5.13-A: Dispersed oil in water flow in pipeline.

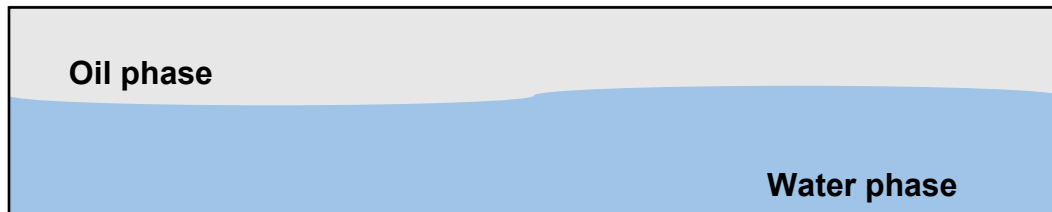


Figure 5.13-B: Stratified oil-water flow in pipeline.

#### 5.3.1.4 Temperature effect

This parameter is very critical since temperature variation leads to variation in all parameters present in the equation.

Starting with the water fluid, many experiments and references showed correlations that water density decrease linearly with temperature, while the Bulk Modulus increases with temperature increase, for the overall effect the SoS in water increases with increasing temperature [54] [55]. Data from these experiments were used in the parametric sensitivity study to understand effect of these parameters.

Regarding the oil fluid, in some experimental papers correlating speed of sound of crude oil or petroleum fluids is done to understand the behaviour of density and SoS of oil when temperature varies [56] [57].

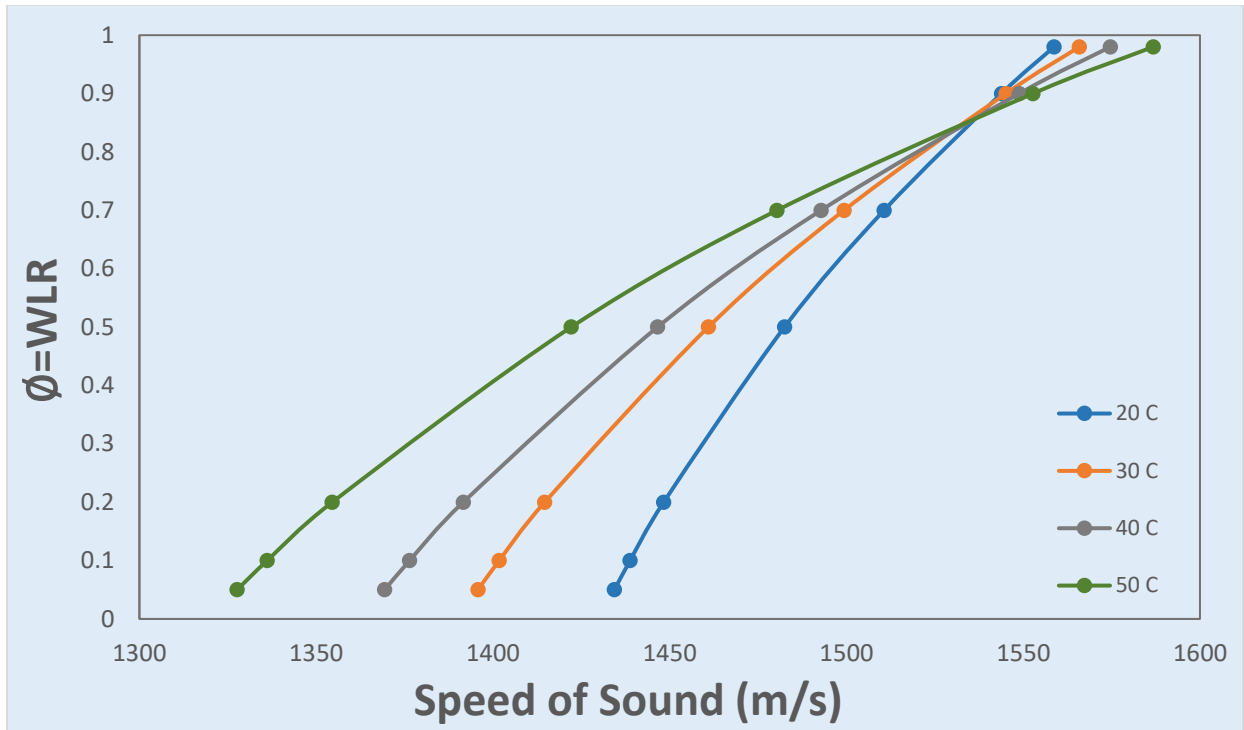


Figure 5.14: Temperature effect on WLR curve versus SoS.

**Trend:**

Dividing the curve for two sections: the first is  $0 \leq \phi \leq 0.85$ , and the second section with condition  $0.85 < \phi \leq 1$ . In the first section, WLR is directly proportional to temperature. While in the second case WLR becomes inversely proportional to temperature. In the first section WLR is very sensitive for temperature and the sensitivity decreases gradually until reaching the end of the first section, then it increases again in the second section.

**Discussion:**

The speed of sound is directly proportional to bulk modulus, and inversely proportional to the density. Increase in temperature leads to decrease in both density and bulk modulus of water, but the order of decrease in density is higher than order in decrease in bulk modulus, hence we observe increase in the speed of sound in case of water, and vice versa in case of oil. Thus in the beginning of the first section, we observe that increase in temperature may lead to very sensitive decrease in the speed of sound, since the

mixture behaves as oil, as the WLR increases the sensitivity decreases gradually until reaching the second section where water composes more than 85% of the mixture flow, the behaviour becomes now similar to water, so the speed of sound increases with temperature increase. This explains the transformation in the trend between both sections.

**5.3.1.5 Pipe thickness effect**

To study the sensitivity of WLR to the pipe thickness “*h*”, the following plot demonstrates different behaviours for different values for *h*.

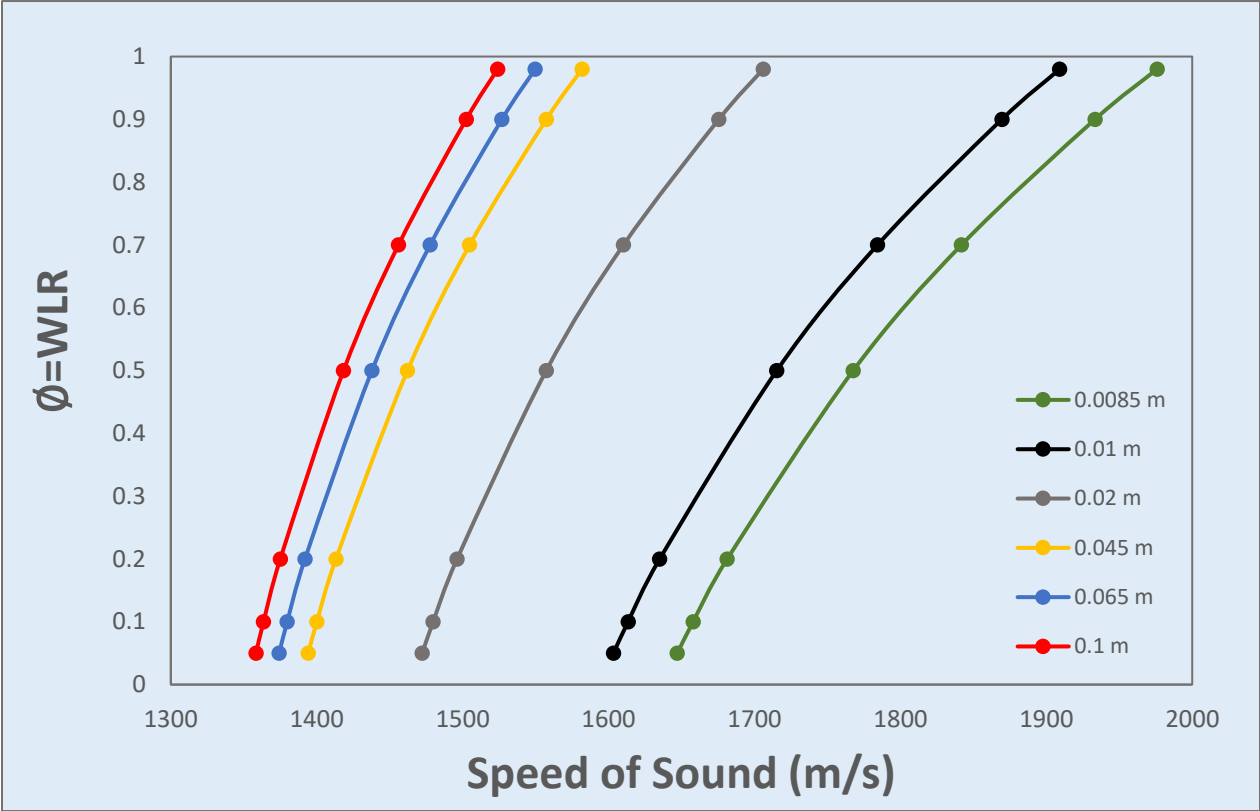


Figure 5.15: Pipe thickness effect on WLR curve versus SoS.

**Trend:**

WLR exhibits a linear proportionality relation with pipe wall thickness, considering small values of *h* it is observed a higher sensitivity of WLR compared to high values of thickness.

### 5.3.1.6 Pipe Young's modulus of elasticity effect

The following plot shows the WLR variation with respect to SoS on the pipe for different values of pipe Young's modulus of elasticity  $E$  presenting a wide range of materials that could be used for pipeline manufacturing.

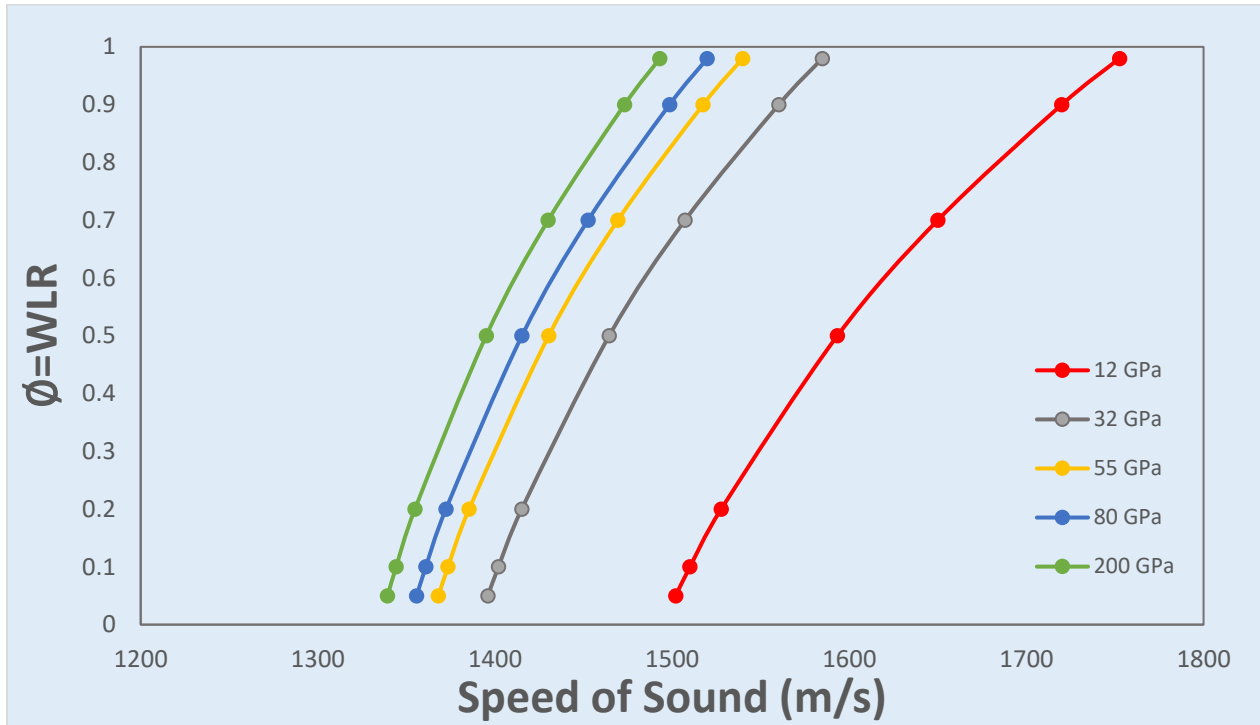


Figure 5.16: Pipe Young's modulus of elasticity effect on WLR curve versus SoS.

#### **Trend:**

As the Young's modulus of pipe increase, WLR increases.

### 5.3.2 Case of Liquid-Gas flow

Considering a Gas-Oil flow, phase fraction is Liquid Holdup ratio defined by:

$$\phi = HL = \frac{V_o}{V_o + V_g} \quad (5.27)$$

Where  $V_o$  and  $V_g$  are the volume of oil and gas respectively. Two parameters are chosen for the sensitivity study including oil density, and temperature.

### 5.3.2.1 Oil density effect

Oil density parameter is also related to oil speed of sound, since its variation also affects the speed of sound as shown in equation 5.24. Range of oil density was [720-980]  $\text{Kg/m}^3$ . The following plot shows the phase fraction variation function of SoS for different oil density values.

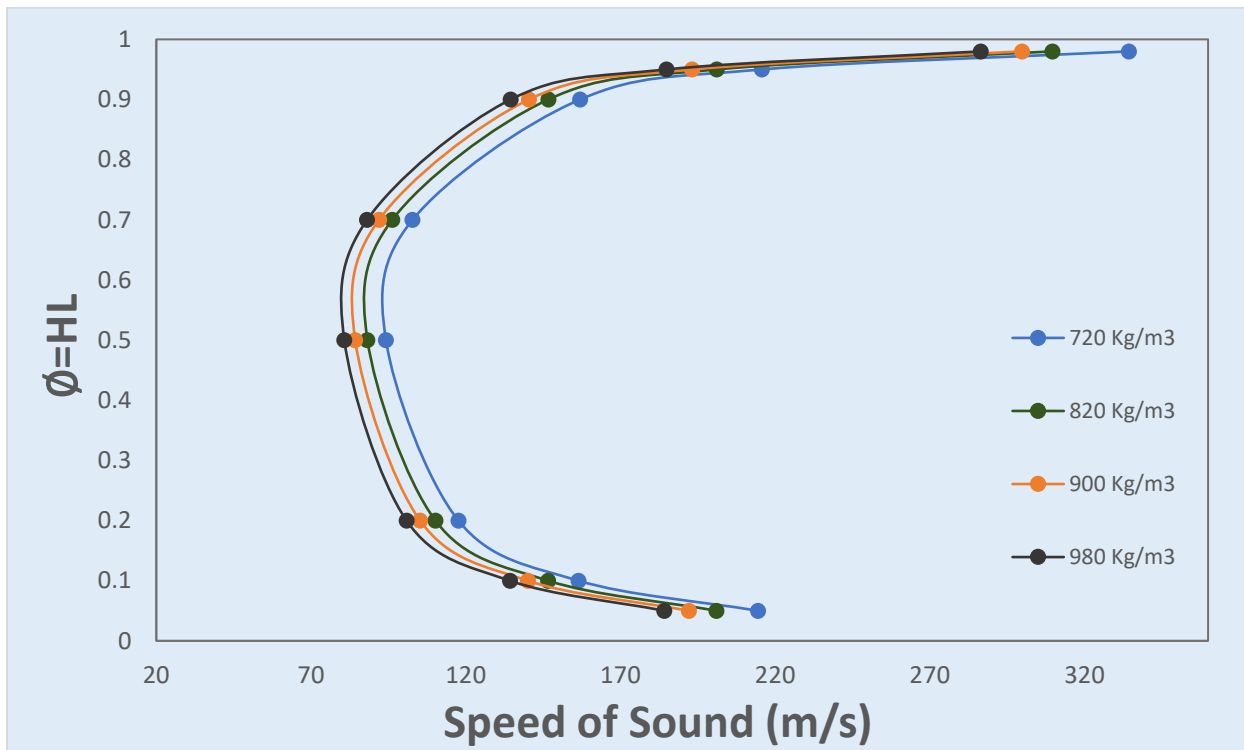


Figure 5.17: Oil density effect on WLR curve versus SoS.

#### **Trend:**

Note that we expect dual solution for  $\phi$  with the correct value depending on the nature of production zones. For Gas-rich flows (low values of  $\phi$ ):  $\phi$  increase as  $\rho_o$  decrease, while for Oil-rich flows (high values of  $\phi$ ):  $\phi$  increase as  $\rho_o$  increase.

**Discussion:**

Considering first solution representing gas-rich flows, the increase in oil density will lead to decrease in the oil phase volume, thus the HL will decrease.

**5.3.2.2 Temperature effect**

As mentioned previously, applying sensitivity study on temperature follows a complex procedure. For oil phase we will refer to the same data of individual phase used in section 5.3.1.3.

Regarding the gas flow acoustic and physical characteristics, the density of gas  $\rho_g$  is determined using the equation state of gases by the equation 5.28:

$$\rho_g = \frac{P}{zRT} \quad (5.28)$$

Where  $P$  is the Pressure,  $z$  is the Compressibility factor,  $R$  is the Specific gas constant,  $T$  is the Temperature.

The SoS in gas  $a_g$  derived from the equation 5.24 to obtain equation 5.29:

$$a_g = \sqrt{\gamma RT} \quad (5.29)$$

Where  $\gamma$  is the Adiabatic constant,  $R$  is the Specific gas constant,  $T$  is the Temperature.

The gas used in this parametric study is Methane gas (Molar Mass 16.04 g/mol) which comprises more than 85% usually of natural gas composition. The following plot shows the phase fraction variation function of SoS for different temperature values.

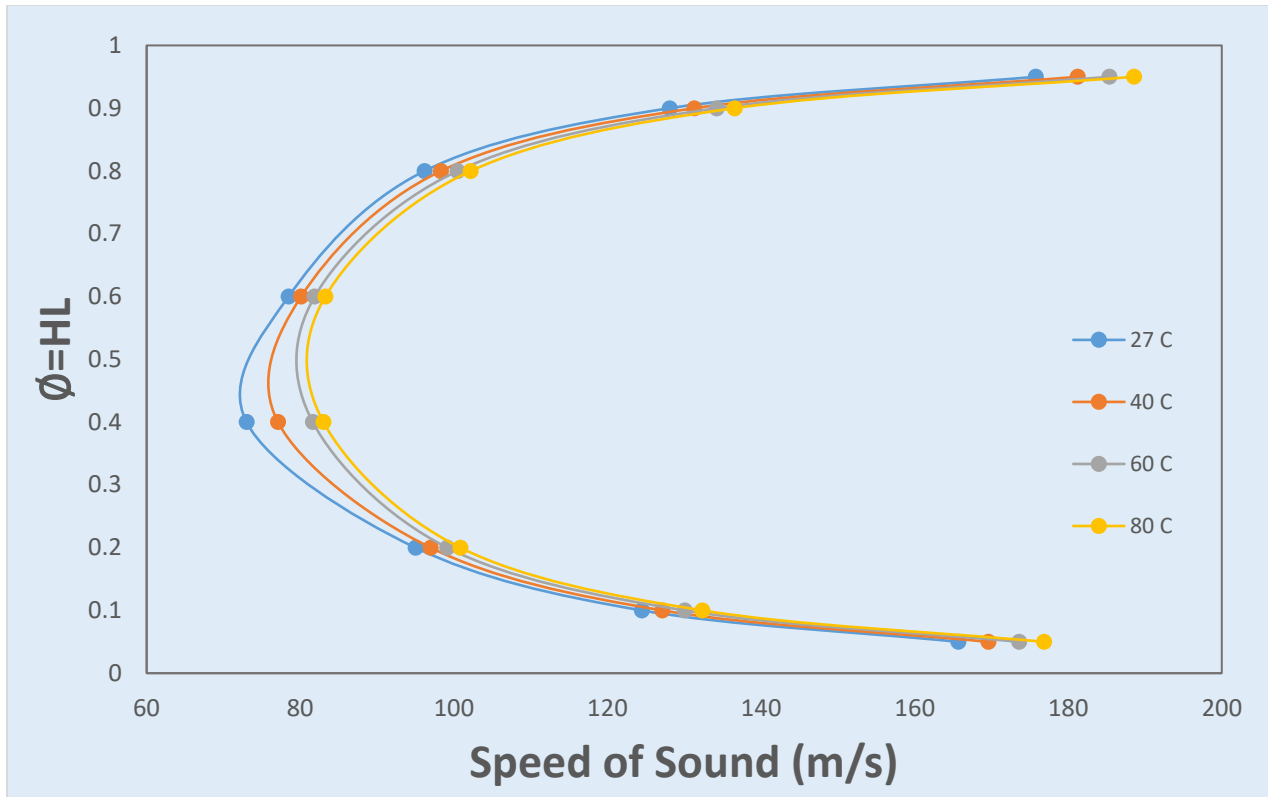


Figure 5.18: Temperature effect on WLR curve versus SoS.

**Trend:**

In the analysis of this liquid-gas flow, the HL always admits two solutions depending on the nature of the flow zone. For Gas-rich flows (low values of  $\phi$ ):  $\phi$  shows a minor unsensitive increase as temperature increase, while for Oil-rich flows (high values of  $\phi$ ):  $\phi$  shows a minor increase as temperature decrease. The only sensitive behaviour of HL to temperature is in HL interval [0.4-0.6], with the rest of the curve show insignificant differences between liquid holdup values.

# **Chapter 6: Proposed Experimental Setup**

A multiphase flow loop is designed with a DAS fiber optic system with the objective of multiphase flow metering to identify flow regimes. The following experiment setup was designed for the multiphase flow lab at Texas A and M University at Qatar, but due to the Covid-19 emergency we could not implement the experiment in the lab, so a proposed experimental setup was developed taking into account detailed description of the components we could use, and applying a risk analysis associated with each component.

## **6.1 Objective**

Creating a multiphase (three phase: liquid-solid-gas) flow loop in order to study different flow regimes of the mixture through a horizontal pipe test section using Distributed Acoustic Sensing (DAS) system.

## **6.2 Experimental Setup**

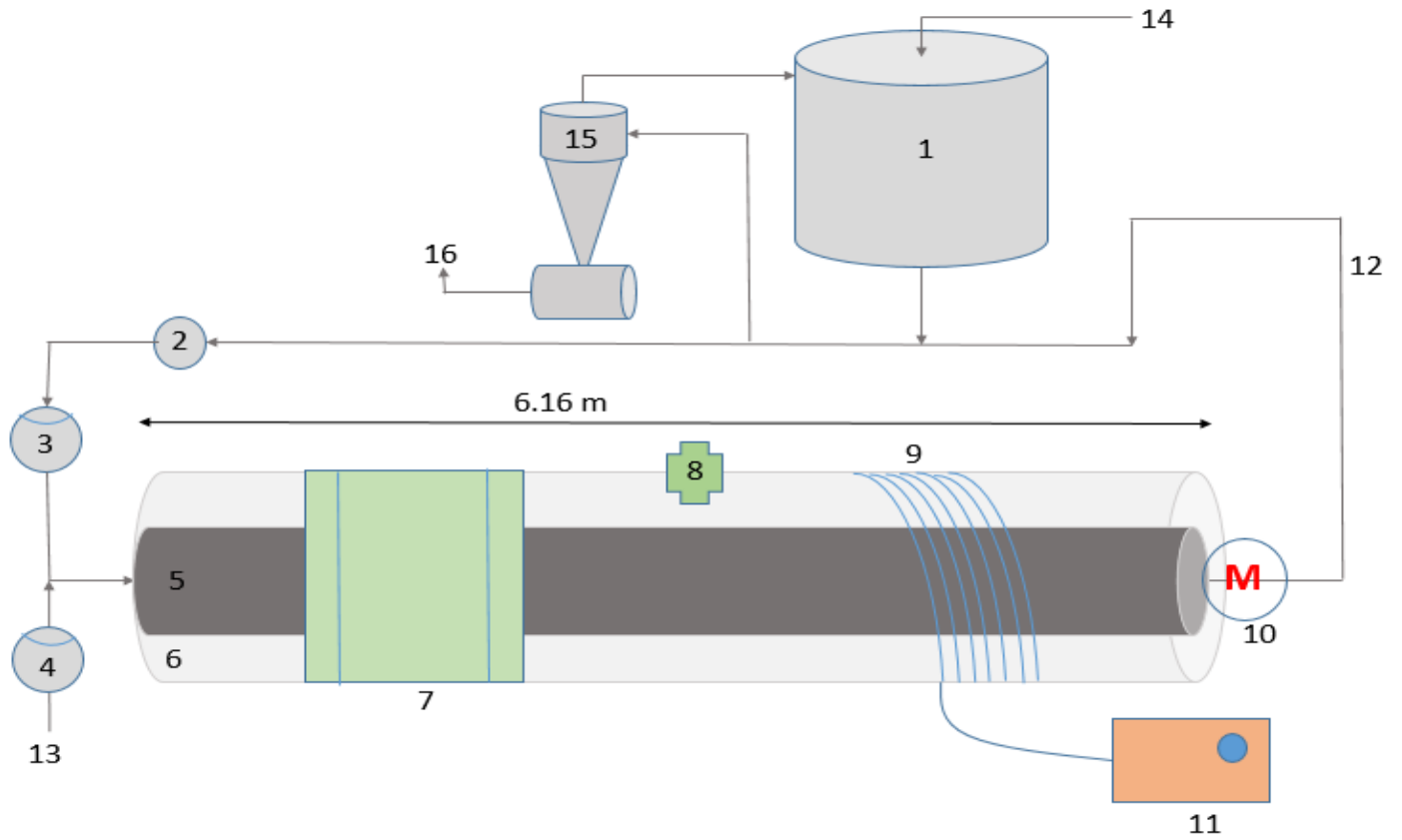


Figure 6.1: Schematic representation of multiphase flow loop.

List of Components of the flow loop:

- 1) Tank
- 2) Pump
- 3) Liquid flow meter
- 4) Gas flow meter
- 5) Inner Pipe
- 6) Outer Pipe
- 7) ERT System
- 8) Eccentricity Regulator
- 9) Fiber Optic Cable
- 10) Motor
- 11) iDAS

- 12) Return line
- 13) Air supply line
- 14) Water inlet
- 15) Hydrocyclone
- 16) Solid outlet

## **6.3 Operating conditions of the system**

The system will be operated with a maximum pressure in the annulus of 1.0 barg (15 psig) when having air-liquid (two phase) flowing in the annulus and 2.0 barg (30 psig) when having only liquid flowing. The system will operate at room temperature.

Solids to be used:

We will use 2-3 mm diameter glass beads as solids at maximum volumetric concentration in the tank of 4%. Glass beads density is about 2600 Kg/m<sup>3</sup>, the solids will be recycled from the hydrocyclone and no dissolution is expected.

Liquids to be used:

Tap water, pH around 7.0. Slurry, consisting of tap water and bentonite, which is clay material, the concentration to be used will vary anywhere between 0.0 to 6.0% by volume and pH around 8.0-9.0.

## **6.4 Description of experimental components**

### **6.4.1 Annulus System**

The proposed experimental setup consists of a 6.16m long annulus of inner and outer pipes. Inner pipe is made up from aluminium with an inner diameter of ID=6.35 cm (2.5 inch), while the outer pipe is made up from a transparent acrylic material with an outer diameter of OD=11.43 cm (4.5 inch).

The inner pipe can be rotated and placed concentrically or eccentrically. The whole unit is set-up on a frame capable of inclination from horizontal to about 15<sup>0</sup> from the

horizontal, to study the effects of inclination. A rotor can rotate the inner tube between 0-150 rpm.

The annulus is set on an aluminium metallic frame of variable height (890mm at horizontal position to a maximum height of 1715 mm at 15° from horizontal), length equal to 6.160 m, and width of 450 mm as shown in figure 6.2. Aluminium is the construction material for the frame and is anodized for extended life. The fasteners provide power locking profile connections of extreme rigidity. It is able to adjust the tilting to the desired degrees driven by a motor. For the bolting of the frame down to the floor 12 screws with 12 mm diameter will be used.

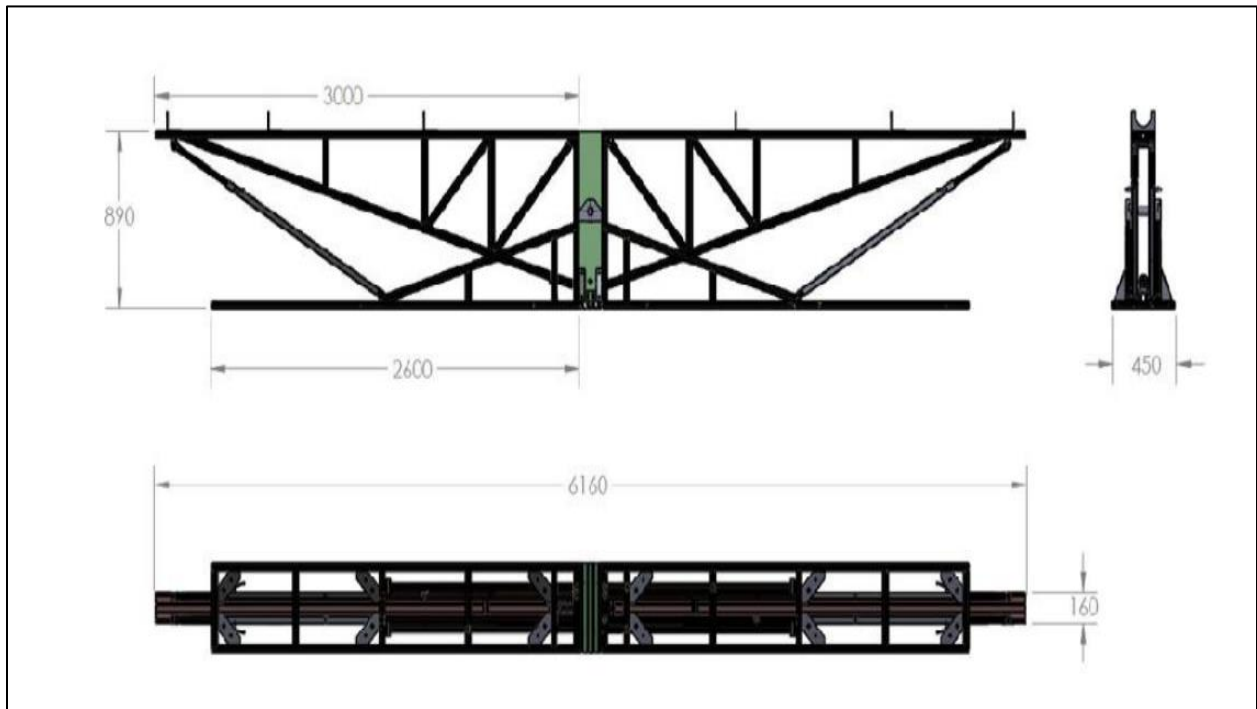


Figure 6.2: Dimensions of aluminium frame (in mm).

### 6.4.2 Pump

Specifications of the slurry pump include a 4 inch input diameter and 2 inch outlet diameter, with the rated power equal to 12.7 KW (17 HP), rated current 20.8 Ampere, and frequency of 60 Hz. Considering the maximum operating conditions, maximum

pressure is 3 barg, and since the maximum velocity in the annulus is 3 m/s then the maximum flow rate is equal to 21.3 l/s.

### 6.4.3 Tank

The system includes a flow tank of 1.0 m<sup>3</sup> capacity (265 gal) equipped with agitator. The tank capacity is 1000 litre. Tank is made up from material INOX AISI304, and the thickness of tank thickness 2mm except for bottom thickness 3mm.

Input diameter is 2 inch, while the output 4 inch, and for drain 2 inch.

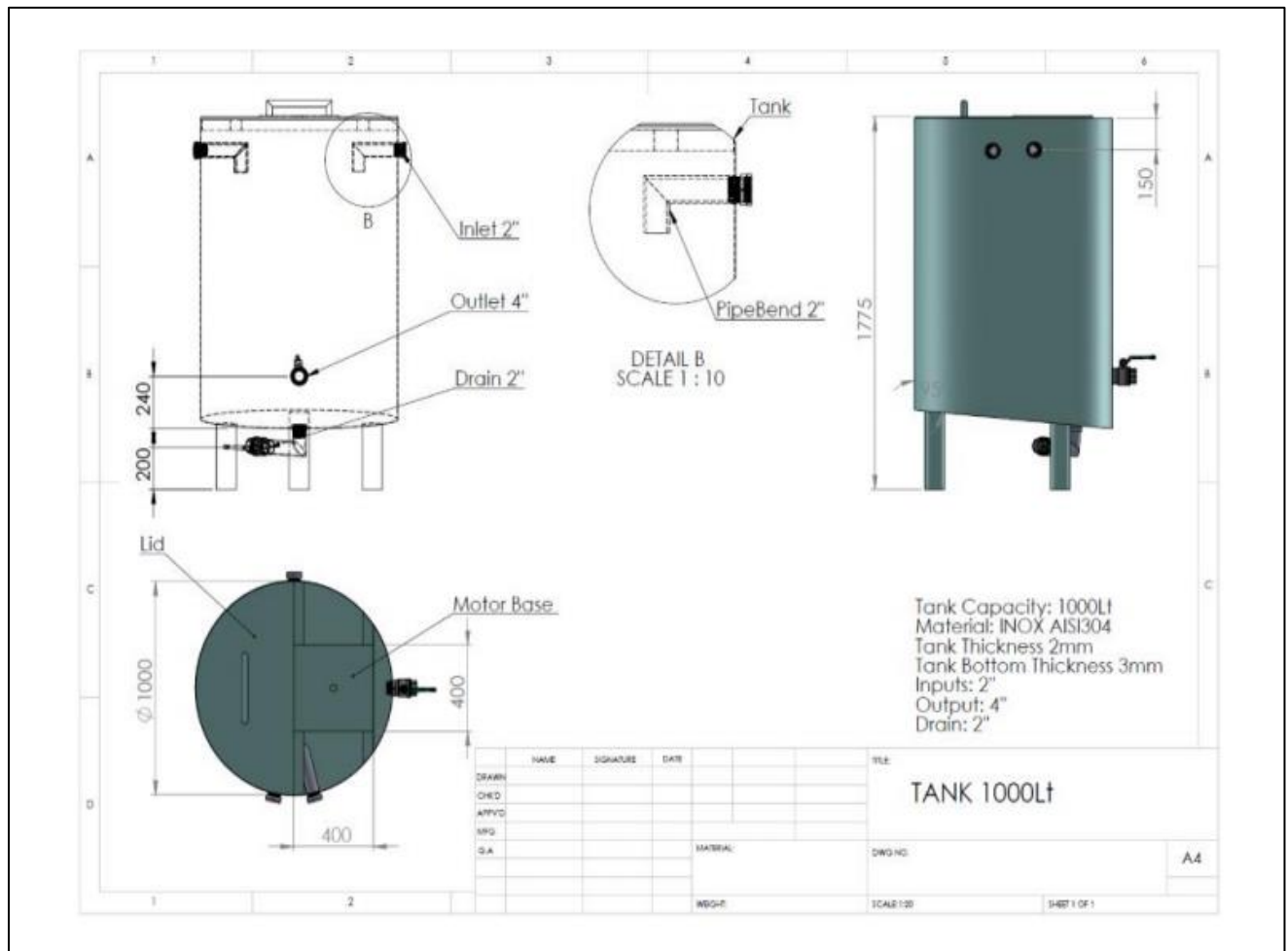


Figure 6.3: Tank design and specifications.

#### 6.4.4 Motor

3- Phase inverter (TOSHIBA) 0.5 HP, 1 KW for tube rotation (10-200 rpm). The motor for rotating the inner tube is 0.18 KW. Inner pipe can also be rotated up to 150 RPM for any eccentric orientation.

#### 6.4.5 Fiber Optic Cable

Fiber optic cable is wrapped helically around a 1.5m section of the annulus as shown in Figure 6.1. A 900  $\mu\text{m}$  diameter of fiber optic which contains a buffer layer to absorb shocks and ensure mechanical protection is chosen. The fiber itself plays the role of sensing element where it can provide a continuous strain profile along the length. Note that both the fiber cable and the iDAS were chosen from Silixa company.

#### 6.4.6 iDAS

The intelligent DAS is an optoelectronic device capable of controlling light signals and detection of backscattered signals due to interaction with acoustic field along the length covered by DAS, where strain induced by acoustic field affect the scattered signals. This device provides a continuous acoustic profile along the length of the fiber optic cable that can reach 40 km, and is applicable with both single mode and multimode fiber optics with no need to utilize any other external device. Its frequency ranges between 1 mHz to 100 kHz, with a high spatial resolution that can reach 1 m, and the dynamic range can exceed 120 dB.



Figure 6.4: iDAS picture [58].

## **6.4.7 Flow meters**

### **6.4.7.1 Liquid flow meter**

Flow Meter Coriolis (liquid), it measures three parameters which are flow rate, density, and temperature. Type of flow meter F200S, 2 inch diameter, and is made up from 316 L stainless steel, 18 to 100 VDC and 85 to 265 VAC, self-switching Analogue flow reading measure with 4-20 mA. Weight of the liquid flow meter is 20 Kg.

### **6.4.7.2 Gas flow meter**

Flow Meter Coriolis (air), it measures three parameters which are flow rate, density, and temperature. Type of flow meter F050S, 0.5 inch diameter, CL150 ASME, and is made up from 316 L stainless steel, 18 to 100 VDC and 85 to 265 VAC, self-switching.

## **6.4.8 Eccentricity Regulator**

The inner pipe can be rotated and placed concentrically or eccentrically. Special designed fasteners are used to secure the frame in position and also allow the system to move in one axis to position it manually eccentric or concentric.

## **6.4.9 Air Supply Line**

Compressed air at room temperature is introduced to the flow from the air supply line with 1 cm diameter before entering the pipe.

## **6.4.10 Hydrocyclone**

The hydrocyclone used will be with 2 inch inlet and 2 inch outlet of INOX material. Flushing at 1.5 bar (2-4 bar operating pressure) from the pump. Safety mechanical relief valve is recommended operating at 2.0 barg.

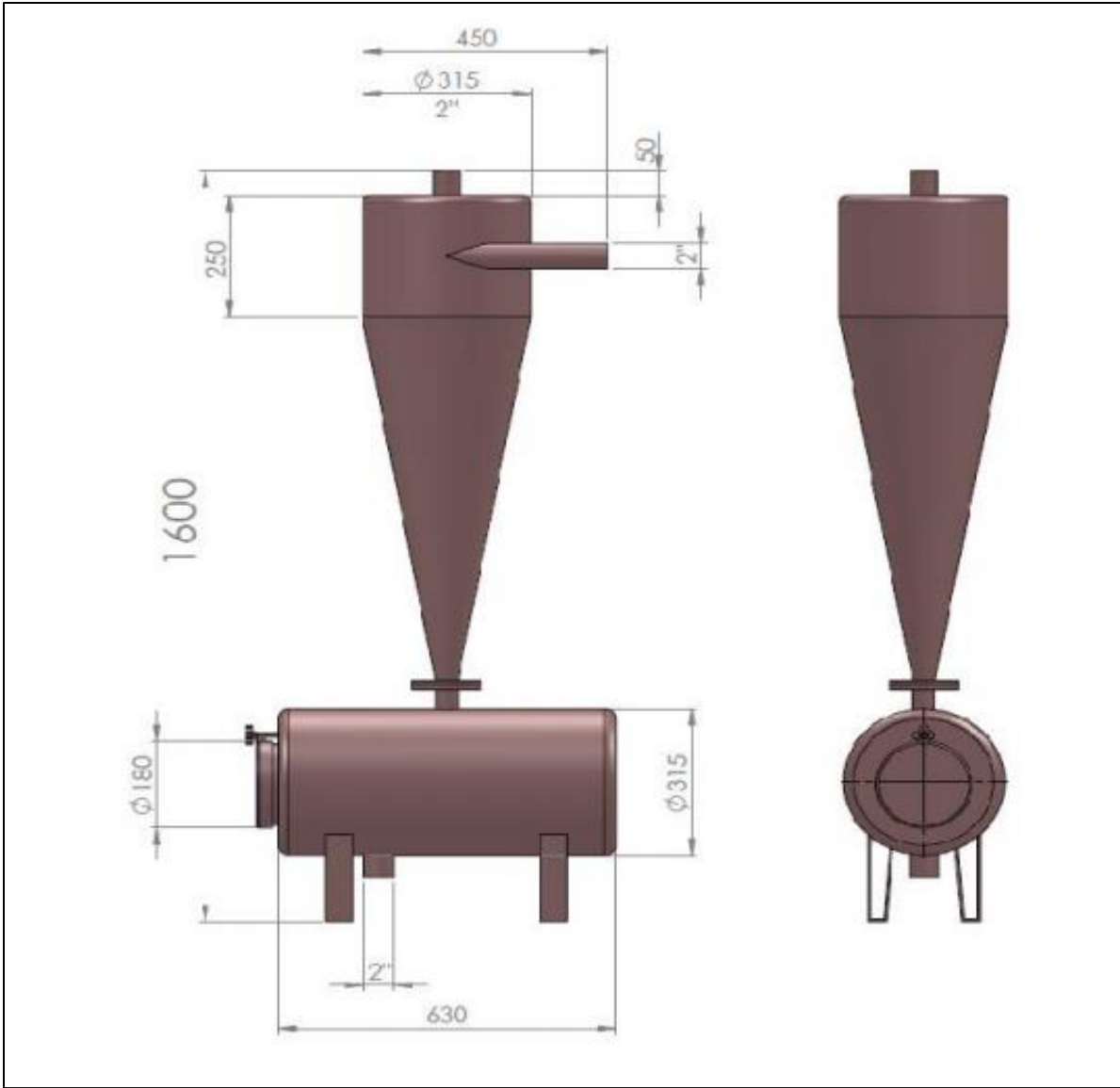


Figure 6.5: Hydrocyclone design specifications.

## 6.5 Risk Analysis

Risk Analysis is the science of assessment and analyzing possible events that can have harmful consequences. The most common technique for risk analysis is the Hazard and Operability Study (HAZOP), which we will perform on our proposed experimental setup according to the criteria that Texas A and M University at Qatar developed which will be presented in the following four tables.

<b>Table 1. Likelihood</b>			
<b>Likelihood (L)</b>	<b>Category</b>	<b>Description</b>	<b>Likelihood as function of number of barriers</b>
Frequent	A	Likely to occur frequently or continuously experienced	No barriers; or only one Administrative or PPE
Probable	B	Will occur several times during life cycle	Only one Engineering; or combination of no more than two Administrative or PPE
Occasional	C	May occur sometime, but rather rarely	Only one Engineering and at least one Administrative or PPE; or at least Administrative or PPE barriers
Remote	D	Unlikely, but possible to occur	At least two Engineering Barriers; or one Engineering, good inherently safer design, and at least one Administrative or PPE
Improbable	E	So unlikely that it can be assumed it will not occur	At least two Engineering Barriers, good inherently safer design and some administrative or PPE

Table 6.1: Likelihood standards.

<b>Table 2. Severity of consequences</b>			
<b>Severity (S)</b>	<b>Category</b>	<b>Description</b>	<b>Examples</b>
Catastrophic	1	Death, life-threatening health effects, permanent serious disability.	Death or paralysis. Leg or hand amputation.
		(Irreversible significant environmental impact.)	
Critical	2	Permanent partial disability, severe injury or illness that may result in long hospitalization or serious health effects that could impair the ability to take protective action.	A deep burn or a major broken bone.
		(Reversible significant environmental impact. Extensive damage to asset.)	Asphyxiation.
Moderate	3	Mild, transient health effects, injury or illness resulting in more than one lost work day and which may require some hospitalizing, but rather short.	Small burn.
		(Reversible significant environmental impact. Minor damage to asset.)	A broken finger or toe.
Marginal	4	Minor injury; injury or illness resulting in no more than one lost work day.	A small cut or twisted ankle.
		(Minimal environmental impact or asset damage.)	

Table 6.2: Severity of consequences standards.

Table 3. Risk Matrix						
		Risk (R)				
Severity (S)	1	1E	1D	1C	1B	1A
	2	2E	2D	2C	2B	2A
	3	3E	3D	3C	3B	3A
	4	4E	4D	4C	4B	4A
		E	D	C	B	A
		Likelihood (L)				

Table 6.3: Risk Matrix.

Table 6.4: Risk acceptance criteria		
<p><b>Acceptable Risk (blue)</b></p> <p>Medium to low risk, which is fully acceptable with periodic review and control.</p>	<p><b>Tolerable Risk (yellow)</b></p> <p>Serious risk, which is tolerable, if demonstrated that is controlled and reduced to ALARP. Make Changes if possible</p>	<p><b>Unacceptable Risk (red)</b></p> <p>High risk, which is not acceptable at any time. Do not Operate. Apply risk reduction measures.</p>
Inspect Annually	Inspect Monthly	Inspect Daily until corrected

Table 6.4: Risk acceptance criteria.

A HAZOP spread sheet was prepared, but in order of simplification, subsystems including their auxiliary equipment are divided into nodes based on their importance. HAZOP can be considered as a holistic study where it merges between complications that lead to decrease in production and other that may cause safety threat to facilities or employees. The multiphase flow loop was divided into a system of 8 different nodes as listed below.

<b>NODE 1</b>	<i>Tank</i>
<b>NODE 2</b>	<i>Hydrocyclone</i>
<b>NODE 3</b>	<i>Pumping system</i>
<b>NODE 4</b>	<i>Liquid flowmeter with supply line</i>
<b>NODE 5</b>	<i>Air supply line with gas flowmeter</i>
<b>NODE 6</b>	<i>DAS system (fiber cable and iDAS)</i>
<b>NODE 7</b>	<i>Pipeline and Motor</i>
<b>NODE 8</b>	<i>Return line</i>

The HAZOP is performed taking into consideration different parameters that are involved in each subsystem taking into account several perspectives the deviation of each parameter, cause, consequence, Severity(S), Likelihood(L), Risk(R) standards, and finally recommendations that can be proposed. For each subsystem or node a table is created summarising all mentioned perspectives as shown below.

Table 6.5: HAZOP on Node 1.

Node 1 : Tank									
Guide Word	Parameter	Deviation	Cause	Consequence	Safeguard	S	L	R	Recommendation
High	Solid content	High solid content	Manual mistake in the required weight of solid	Corrosion	Administration control	3	C	3C	Regular inspection
				Improper function of the pump		2	B	2B	Strainer or filter before pump suction must be installed
High	Mixing	High Mixing	Failure of the agitator	Temperature rise	-	3	C	3C	Speed sensor must be installed to monitor agitation process
				Vortex formation and erosion		3	D	3D	
High	Pressure	High pressure	Outlet blockage/ Valve closed	Tank rupture and explosion	Engineering control	1	C	1C	Pressure gauge installation
			Exterior fire	Leakage from tank		2	D	2D	
Low		Low pressure	High suction rate from tank	Improper flow rates out of tank		4	C	4C	

High	Temp-erature	High temp-erature	High ambient temperature	Explosion	-	1	C	1C	Install temperature sensor
			High tank pressure	Leakage		2	D	2D	
Low		Low temp-erature	Low ambient temprature	Extremely low temperature cause improper flow out the tank	At least 1°C	3	D	3D	
High	Flow	More flow	Increase flow from inlet	Excessive fluid level in tank	Engineering control	2	D	2D	Flow control to the feed
Low		Less flow	Less feed in inlet	Decrease in storage capacity		4	D	4D	Proper Maintenance and checking of line
No		No flow	Blockage in inlet line	Damage in the pump		2	D	2D	
More	Level	More level	Failure of level indicator	Possible pressure increase	-	2	C	2C	Level indicator installation
Less		Less level	Damage in equipement	Integrity loss causing rupture	-	2	C	2C	
	Failure of control valve		Excessive outlet flow	3		D	3D		
High	PH	High PH	Manual error in feed PH	Corrosion and equipment cracking	Engineering control	1	C	1C	PH sensor to be provided

Table 6.6 HAZOP on Node 2.

Node 2 : Hydrocyclone									
Guide Word	Parameter	Deviation	Cause	Consequence	Safeguard	S	L	R	Recommendation
Sudden change	Pressure	Sudden Change in pressure	Inlet flow rate change	Cut point change	Engineering control	2	D	2D	Pressure sensor installation
Low		Low pressure	Leakage	Poor separation		3	D	3D	
High	Feed density	High feed density	High solid volume concentration	Performance reduction	Adminstration control	4	C	4C	-
Low	Temperature	Low temperature	Low ambient temperature	Poor separation	Engineering control	3	D	3D	Temperature sensor installation

Table 6.7: HAZOP on Node 3.

Node 3 : Pumping system										
Guide Word	Parameter	Deviation	Cause	Consequence	Safeguard	S	L	R	Recommendation	
High	Pressure	High pressure	Leakage	Damage in supply line with rupture risk	Engineering control	1	B	1B	Installation of a pressure gauge	
Low		Low pressure	Operation plug	Pump performance reduction		3	D	3D		
			Fluid entry at low pressure	Cavitation and excessive vibration		1	B	1B	Impeller inducer installation	
More		Flow	More flow	High fluid pressure at inlet		Damage in the filter	Administration control	3	C	3C
				Turbulence/ Excessive vibration	2	B		2B		
Less	Less flow		Clogged suction	Performance reduction	Cavitation	3		D	3D	Impeller inducer installation
								1	B	
No	No flow	Blockage of inlet line	Pump damage		2	D	2D	Regular inspection		

High	Temperature	High temperature	Inlet fluid with high temperature	Pressure incrementation in transportation line	Engineering control	2	D	2D	Temperature sensor installation
Low		Low temperature	Inlet fluid with low temperature	Performance reduction		3	D	3D	

Table 6.8: HAZOP on Node 4.

Node 4 : Liquid flowmeter with supply line									
Guide Word	Parameter	Deviation	Cause	Consequence	Safeguard	S	L	R	Recommendation
High	Pressure	High pressure	High flow rate	Damage to supply line	-	2	C	2C	Pressure gauge
Low		Low pressure	leakage	Poor performance		3	B	3B	
High	Temperature	High Temperature	High ambient Temperature	Flowmeter damage	Engineering control	2	C	2C	Temperature sensor installation
				Supply line rupture		1	C	1C	
Low		Low Temperature	Low Temperature	Performance reduction		4	D	4D	

More	Flow	More flow	Improper function of pump	Pressure increase	Engineering control	2	C	2C	Flow detector implementation
Less		Less flow	Leakage	Low pressure supply		3	D	3D	
No		No flow	Line blockage	Line supply rupture		1	C	1C	Regular inspection

Table 6.9: HAZOP on Node 5.

Node 5 : Air supply line with gas flowmeter									
Guide Word	Parameter	Deviation	Cause	Consequence	Safeguard	S	L	R	Recommendation
High	Pressure	High pressure	System roughness	Condensate formation	-	2	C	2C	Utilization of water trap and filter regulator
Low		Low pressure	leakage	Poor performance		3	B	3B	-
More	Flow	More flow	Malfunction of air supply line	Pressure increase	Engineering control	2	C	2C	Flow detector implementation

Less		Less flow	Leakage	Low pressure supply		3	D	3D	
No		No flow	Line blockage	Line supply rupture		1	C	1C	Regular inspection
			Air supply line shutdown	Flowmeter damage		2	D	2D	

Table 6.10: HAZOP on Node 6.

Node 6 : DAS system (fiber cable and iDAS)									
Guide Word	Parameter	Deviation	Cause	Consequence	Safeguard	S	L	R	Recommendation
Off	Power	Power failure	Electric shutdown	iDAS damage	-	1	B	1B	Uninterruptible power source (UPS) installation
				DAS data loss	Engineering control	2	B	2B	
Cut	Fiber	Fiber cut	Natural forces	Core break with Optical signal loss	Administration control	1	D	1D	Maintainance improving
			Accident			1	C	1C	Worker training on fiber optics
			External Fire			1	C	1C	Fire protection system

Table 6.11: HAZOP on Node 7.

Node 7 : Pipeline and Motor									
Guide Word	Parameter	Deviation	Cause	Consequence	Safeguard	S	L	R	Recommendation
More	Flow	More flow	High supply flow rate	Motor damage	Engineering control	2	C	2C	Flow detector utilization.
			Pipeline rupture	1		C	1C		
Less flow		Leakage	Missleading flow patterns in test section	4		D	4D		
No flow		Supply blockage	Motor damage	2		C	2C		
High	Temperature	High Temperature	High ambient temperature	Pipeline rupture	Engineering control	1	C	1C	Temperature sensor installation
			Motor failure	2		C	2C		
Low		Low Temperature	Low ambient temperature	Performance reduction		4	D	4D	
Off	Power	Power failure	Electric shutdown	Motor damage	-	1	B	1B	Uninterruptible power source (UPS) installation
			Motor failure	Pipe can no more be inclined	-	3	D	3D	

High	Pressure	High pressure	High pipe outlet pressure	Motor failure	Engineering control	2	D	2D	Pressure sensor installation
			High supply pressure	Pipe Damage		2	C	2C	

Table 6.12: HAZOP on Node 8.

Node 8 : Return line									
Guide Word	Parameter	Deviation	Cause	Consequence	Safeguard	S	L	R	Recommendation
More	Flow	More flow	High supply pressure	Pipe failure	Engineering control	3	C	3C	Flow detector after the motor directly.
				Leakage		2	D	2D	
No		No flow	Pipe rupture	Flow leakage		3	C	3C	
			Supply failure	Stop of flow circulation		4	D	4D	
Less		Less flow	Pipe leakage	Loss of mixture flow		3	C	3C	
			Low supply pressure	Low pressure in the pipeline test section		4	D	4D	

High	Pressure	High pressure	High supply pressure	Pipe rupture	Engineering control	2	B	2B	Pressure sensor installation
Low		Low pressure	Low supply pressure	Circulation performance reduction		4	C	4C	
High	Temperature	High temperature	High ambient temperature	Supply line failure	Engineering control	1	D	1D	Temperature sensor installation
			Turbulence effects	Pressure increase in system		3	C	3C	
Low		Low temperature	Low ambient temperature	Freezing of pipeline		2	C	2C	

# Chapter 7: Conclusion

## 7.1 Discussion and Conclusion

Distributed Fiber Optic Sensing (DFOS) is a powerful tool for the task of multiphase flow metering in pipelines. Its distinguished properties enabled the production of various applications in all petroleum industry sectors including exploration to production and transportation, with the focus of this paper on pipeline monitoring.

Through a review on publications present in this domain, it was notable the lack of three phase flow condition in DFOS experiments, with the ability to study two phase flow patterns such as bubbly, churn, or annular flow is always discussed especially in small diameter pipes.

Speed of Sound (SoS) is clearly demonstrated how to be extracted using one of the promising techniques of DFOS that is the Distributed Acoustic Sensing (DAS) including all steps of signal processing ending with the two dimensional Fourier transform applied to time-space domain producing a V-shape in the frequency-wavenumber space. Then linking this measured SoS of the mixture to individual phase fractions and volumetric flow rates is shown, before finally studying the variation of phase fraction to different parameters using a parametric sensitivity, where the first case is on a liquid-liquid flow we obtained the following conclusions regarding Water in Liquid Ratio (WLR):

- WLR is directly proportional to oil density, pipe thickness, pipe Young's modulus of elasticity, and temperature in case of  $WLR \leq 0.8$
- WLR is inversely proportional to the bulk modulus of oil, pipe diameter, and temperature in case of  $WLR > 0.8$

On the other hand, the Liquid Holdup (HL) in case of liquid-gas flow, the oil density and the temperature.

- HL is inversely proportional to oil density in gas-rich flow regimes, while it is directly proportional to oil density in case of oil-rich flows.

- HL is directly proportional to temperature in gas-rich flow regimes, while it is inversely proportional to temperature in case of oil-rich flows. HL is slightly sensitive to temperature, very small variations occur when temperature varies.

A proposed experimental setup was designed to be applied at Texas A and M at Qatar University using Distributed Acoustic Sensing (DAS) on a 2.5 inch inner diameter annular pipe with 6.16 m length to simulate a multiphase flow, with the maximum operating pressure is 1 barg for liquid-gas flow and 2 barg for liquid-liquid flow. An overview of the components used is done with their specifications present. Varying the superficial velocities of the fluids we can thus visualize different multiphase flow regimes that enable us to build a flow regime map, which can be compared to ones present in the literature to validate the results. Eventually we performed a HAZOP risk analysis is done for different components of the system, to evaluate safety conditions of the experiment according to the standards of Texas A and M at Qatar University. Due to the Covid-19 emergency we were not able to perform the experiment, so the design will be used by the research team in multiphase flow laboratory when the laboratory reopens.

## **7.2 Future Work Recommendations**

Regarding future work, it is recommended the following:

- Creating Artificial Neural Network to apply machine learning using a programming language such as Matlab or Python to train the network to recognize the flow pattern or regime from huge experimental data.
- Performing experimental tests using DAS on multiphase flow changing both pipe material and thickness to validate the results obtained; the experiment could be done on three phase mixture trying to obtain a new correlation of speed of sound with phase fraction for more than two phases.
- Experimentally, study the effect of temperature on the phase fractions of both liquid-liquid and liquid-gas flow to understand or validate the complex behaviour under increasing temperature.

# References

- [1] D. Finfer, T. R. Parker, V. Mahue, M. Amir, M. Farhadiroushan and S. Shatalin, "Non-intrusive Multiple Zone Distributed Acoustic Sensor Flow Metering," in *SPE Annual Technical Conference and Exhibition*, Houston, Texas, USA, 2015.
- [2] Ö. H. Ünalmsis, "The use of sound speed in downhole flow monitoring applications," *The Journal of the Acoustical Society of America*, vol. 137, no. 4, pp. 2224-2224, April 2015.
- [3] D. B. Foo, J. Krislock, T. J. Meador and T. Cheng, "Horizontal Well Injection Profiling Using Distributed Temperature Sensing," in *SPE/CSUR Unconventional Resources Conference*, Calgary, Alberta, Canada, 2014.
- [4] O. Fidaner, "Downhole Multiphase Flow Monitoring Using Fiber Optics," in *SPE Annual Technical Conference and Exhibition, 9-11 October*, San Antonio, Texas, USA, 2017.
- [5] O. H. Unalmsis and S. Trehan, "Downhole Multiphase Flow Measurement in Horizontal Wellbores," in *EAGE Annual Conference & Exhibition incorporating SPE Europec, 10-13 June*, London, UK, 2013.
- [6] G. Feo, J. Sharma, . W. Williams, . D. KortuKov and . O. Toba, "Application of Distributed Fiber Optics Sensing Technology for Real-Time Gas Kick Detection," in *SPE Annual Technical Conference and Exhibition*, Calgary, Alberta, Canada, 2019.
- [7] B. D. Carnahan, R. W. Clanton, K. D. Koehler, G. O. Harkins and G. R. Williams, "Fiber Optic Temperature Monitoring Technology," in *SPE Western Regional Meeting*, Anchorage, Alaska, 1999.
- [8] P. Webster, J. Wall, C. Perkins and M. Molenaar, "Micro-Seismic Detection Using Distributed Acoustic Sensing," in *2013 SEG Annual Meeting*, Houston, Texas, 2013.
- [9] S. Addanki, P. Yupapin and I. S. Amiri, "Review of optical fibers-introduction and applications in fiber lasers," *Results in Physics*, vol. 10, pp. 743-750, September 2018.
- [10] R. D. Sante, "Fibre Optic Sensors for Structural Health Monitoring of Aircraft Composite Structures: Recent Advances and Applications," *Sensors*, pp. 18666-18713, 15 August 2015.
- [11] V. Kouhdaragh , D. Tarchi, A. Vanelli-Coralli and G. E. Corazza, "Smart Grid Inspired Future Technologies," 2017.
- [12] X. Zhou, Z. Chen, J. Hou and H. Zhou, "Mode-field adaptor between large-mode-area fiber and single-mode fiber based on fiber tapering and thermally expanded core technique," *Applied Optics*, August 2014.

- [13] W. Wang, L. Yang, T. Jiang and Q. Zhang, "Configurations and Diagnosis for Ultra-Dense Heterogeneous Networks: From Empirical Measurements to Technical Solutions," *IEEE Network*, vol. 32, no. 3, pp. 138-145, May/June 2018.
- [14] A. Ghosh and P. K. Paul, "Alignment considerations in extrinsic fiber-optic sensors," *Applied Optics*, vol. 36, no. 25, pp. 6256-6263, October 1997.
- [15] P. M. Tracey, "Intrinsic Fiber-optic Sensors," *IEEE Transactions on Industry Applications*, vol. 27, no. 1, pp. 96-98, January/February 1991.
- [16] M. Amanzadeh, S. M. Aminossadati, M. S. Kizil, S. Aminossadati and A. D. Rakić, "Recent developments in fibre optic shape sensing," *Measurement*, vol. 128, pp. 119-137, 2018.
- [17] Z. Qian, M. Zhang, J. Li, Y. Xu, T. Wang, L. Qiao, J. Zhang and M. Promi, "High-accuracy distributed temperature measurement using difference sensitive-temperature compensation for Raman-based optical fiber sensing," *Optics Express*, vol. 27, no. 25, pp. 36183-36196, December 2019.
- [18] J. P. Dakin, D. J. Pratt, J. N. Ross and G. W. Bibby, "Distributed optical fibre Raman temperature sensor using a semiconductor light source and detector," *Electronics Letters*, vol. 21, no. 13, pp. 569-570, 20 June 1985.
- [19] T. Shiota and F. Wada, "Distributed temperature sensors for single-mode fibers," in *Proceedings of SPIE*, 1992.
- [20] A. Mishra, S. H. Al Gabani and A. Jumaa Al Hosany, "Pipeline Leakage Detection Using Fiber Optics Distributed Temperature Sensing DTS," in *Abu Dhabi International Petroleum Exhibition & Conference*, Abu Dhabi, UAE, 2017.
- [21] A. Zrelli, T. Ezzedine and B. Mohamed, "Measurement of Temperature through Raman Scattering," *Procedia Computer Science*, vol. 73, pp. 350-357, 2015.
- [22] D. Belanger and L.-B. Ouyang, "Flow Profiling via Distributed Temperature Sensor (DTS) System - Expectation and Reality," in *SPE Annual Technical Conference and Exhibition*, Houston, Texas, 2004.
- [23] X. Bao, J. Dhliwayo, N. Heron, D. J. Webb and D. A. Jackson, "Experimental and theoretical studies on a distributed temperature sensor based on Brillouin scattering," *Journal of Lightwave Technology*, vol. 13, no. 7, pp. 1340-1348, 1995.
- [24] M. Farhadiroushan, T. R. Parker, R. Feced, A. J. Rogers and V. A. Handerek, "Simultaneous distributed measurement of strain and temperature from noise-initiated Brillouin scattering in optical fibers," *IEEE Journal of Quantum Electronics*, vol. 34, no. 4, pp. 645-659, 1998.
- [25] D. A. Jackson, C. N. Panell, F. Farahi and D. Culverhouse, "Potential of stimulated Brillouin scattering as sensing mechanism for distributed temperature sensors," *Electronics Letters*, vol. 25, no. 14, pp. 913-915, 1989.

- [26] K. Shmizu, T. Horiguchi and Y. Koyamada, "Measurement of distributed strain and temperature in a branched optical fiber network by use of Brillouin optical time-domain reflectometry," *Optics Letters*, vol. 20, no. 5, pp. 507-509, 1995.
- [27] D. Garcus, T. Gogolla, K. Krebber and F. Schliep, "Brillouin optical-fiber frequency-domain analysis for distributed temperature and strain measurements," *Journal of Lightwave Technology*, vol. 15, no. 4, pp. 654-662, 1997.
- [28] A. K. Sang, M. E. Froggatt, D. Gifford, S. T. Kreger and B. D. Dickerson, "One Centimeter Spatial Resolution Temperature Measurements in a Nuclear Reactor Using Rayleigh Scatter in Optical Fiber," *IEEE Sensors Journal*, vol. 8, no. 7, pp. 1375-1380, 2008.
- [29] M. Li, H. Wang and G. Tao, "Current and Future Applications of Distributed Acoustic Sensing as a New Reservoir Geophysics Tool," *The Open Petroleum Engineering Journal*, vol. 8, no. 1, pp. 272-281, 2015.
- [30] F. Aminzadeh and R. T. Cannon, "Distributed Acoustic Sensing: State of the Art," in *SPE Digital Energy Conference*, Texas, USA, 2013.
- [31] A. Mateeva, J. Lopez, J. Mestayer, P. Wills, B. Cox, D. Kiyashchenko, Z. Yang, W. Berlang, R. Detomo and S. Grandi, "Distributed acoustic sensing for reservoir monitoring with VSP," in *76th EAGE Conference and Exhibition - Workshops*, 2014.
- [32] Y. S. Muanenda, "Recent Advances in Distributed Acoustic Sensing Based on Phase-Sensitive Optical Time Domain Reflectometry," *Journal of Sensors*, pp. 1-16, May 2018.
- [33] A. Mendez and E. Diatzikis, "Fiber Optic Distributed Pressure Sensor Based on Brillouin Scattering," in *Proceedings Optical Fiber Sensors*, Mexico, 2006.
- [34] T. Chen, Q. Wang, R. Chen, B. Zhang, C. Jewart, K. P. Chen, M. Maklad and P. R. Swinehart, "Distributed high-temperature pressure sensing using air-hole microstructural fibers," *Optics letters*, vol. 37, no. 6, pp. 1064-1066, 15 March 2012.
- [35] K. Kalar, "Fiber Optics Aim to Improve Leak Monitoring With Distributed Temperature Sensing," *Pipeline & Gas Journal*, May 2008.
- [36] B. Eisler and G. A. Lanan, "Fiber Optic Leak Detection Systems for Subsea Pipelines," in *Offshore Technology Conference*, Houston, Texas, USA, 2012.
- [37] R. Kluth, D. Watley, H. Vogel and K. Yoosung, "Leak Detection For Pipelines Using Distributed Fibre Optic Sensors," in *Offshore Mediterranean Conference and Exhibition*, Ravenna, Italy, 2007.
- [38] S. Grayson, Y. Gonzalez, K. England, R. Bidyk and S. F. Pitts, "Monitoring Acid Stimulation Treatments in Naturally Fractured Reservoirs with Slickline Distributed Temperature Sensing," in *SPE/ICoTA Coiled Tubing & Well Intervention Conference & Exhibition*, Texas, USA, 2015.

- [39] B. Xu and . F. Forouzanfar, "Uncertainty Reduction in Reservoir Geostatistical Description Using Distributed Temperature Sensing (DTS) Systems Data," in *SPE Western Regional Meeting*, Anchorage, Alaska, USA, 2016.
- [40] F. Zaini and D. Keough, "Downhole Remote Monitoring System for SAGD Observation Wells through Fiber Optic DTS," in *SPE Canada Heavy Oil Technical Conference*, Calgary, Alberta, Canada, 2017.
- [41] M. Rahman, P. J. Zannitto, D. A. Reed and M. E. Allan, "Application of Fiber-Optic Distributed Temperature Sensing Technology for Monitoring Injection Profile in Belridge Field, Diatomite Reservoir," in *SPE Digital Energy Conference and Exhibition*, Texas, USA, 2011.
- [42] D. Denney, "Flow Profiling Gas Wells With Distributed-Temperature-Sensing Data," *Journal of Petroleum Technology*, vol. 59, no. 4, pp. 67-70, April 2007.
- [43] R. Paleja, D. Mustafina, T. Park, D. Randell, Peter in 't panhuis, R. I. Crickmore and J. van der Horst, "Velocity Tracking for Flow Monitoring and Production Profiling Using Distributed Acoustic Sensing," in *SPE Annual Technical Conference and Exhibition*, 2015.
- [44] J. Mestayer , B. Cox , P. Wills, D. Kiyashchenko, J. Lopez, M. Costello, G. Ugueto, R. Lupton, G. Solano, S. Bourne, D. Hill and A. Lewis, "Field Trials of Distributed Acoustic Sensing For Geophysical Monitoring," in *2011 SEG Annual Meeting, 18-23 September*, San Antonio, Texas, 2011.
- [45] M. M. Molenaar, D. Hill , P. Webster, E. Fidan and B. Birch, "First Downhole Application of Distributed Acoustic Sensing for Hydraulic-Fracturing Monitoring and Diagnostics," *SPE Drilling & Completion*, vol. 27, no. 1, pp. 32 - 38, March 2012.
- [46] F. Hveding and A. Bukhamsin, "Distributed Fiber Optic Sensing – A Technology Review for Upstream Oil and Gas Applications," in *SPE Kingdom of Saudi Arabia Annual Technical Symposium and Exhibition*, Dammam, Saudi Arabia, 2018.
- [47] C. Allanic, J. Frangeul, M. Liebeck, B. Carbonnier, G. J. Naldrett, M. Farhadiroushan and A. Clarke, "Distributed Acoustic Sensing For ESP Understanding And Surveillance," in *SPE Middle East Intelligent Energy Conference and Exhibition*, Manama, Bahrain, 2013.
- [48] G. Hemink and J. van der Horst, "On the Use of Distributed Temperature Sensing and Distributed Acoustic Sensing for the Application of Gas Lift Surveillance," *SPE Production & Operations*, vol. 33, no. 4, pp. 896 - 912, 2018.
- [49] T. Williams, E. Lee, J. Chen, X. Wang, D. Lerohl, G. Armstrong and Y. Hilts, "Fluid Ingress Location Determination Using Distributed Temperature and Acoustic Sensing," in *SPE Digital Energy Conference and Exhibition*, The Woodlands, Texas, USA, 2015.
- [50] W. Assiri, I. Uzun and E. Ozkan, "Distributed Pressure Sensing for Production Data Analysis," in *SPE Middle East Oil and Gas Show and Conference, 18-21 March*, Manama, Bahrain, 2019.

- [51] F. F. Zinati, M. D. Jansen and S. M. Luthi, "Estimating Near-Wellbore Permeability by Distributed Pressure Sensing Using an Adjoint-Based Minimization Algorithm," in *SPE Annual Technical Conference and Exhibition*, Florence, Italy, 2010.
- [52] A. B. Wood, A textbook of sound, 1941.
- [53] L. M. Al-Hadhrami, S. M. Shaahid, L. O. Tunde and A. Al-Sarkhi, "Experimental Study on the Flow Regimes and Pressure Gradients of Air-Oil-Water Three-Phase Flow in Horizontal Pipes," *The Scientific World Journal*, 2014.
- [54] M. Tanaka, G. Girard, R. Davis and A. Peuto, "Recommended table for the density of water between 0 °C and 40 °C based on recent experimental reports," *Metrologia*, vol. 38, no. 4, 2001.
- [55] D. V. d. Sompel, L. S. Sasportas, A. Dragulescu-Andrasi and S. E. Bohndiek, "Improving Image Quality by Accounting for Changes in Water Temperature during a Photoacoustic Tomography Scan," *PLOS One*, vol. 7, no. 10, October 2012.
- [56] H. H. Dashti and M. R. Riazi , "Acoustic velocities in petroleum fluids: Measurement and prediction," *Journal of Petroleum Science and Engineering*, vol. 124, pp. 94-104, 2014.
- [57] M. Vakilinejad, J. Xia, R. S. A-Maamari, N. Al-Rawahi and G. Vakili-Nezhaad, "Density Correlation of Some Pure Hydrocarbons and Crude Oil Samples with the Speed of Sound," in *International Conference on Machine Learning, Electrical and Mechanical Engineering (ICMLEME'2014)*, Dubai (UAE), 2014.
- [58] Silixa, "intelligent Distributed Acoustic Sensor (iDAS™)," No date. [Online]. Available: <https://silixa.com/products/idas/>. [Accessed 28 8 2020].